

Structure of the *Chlamydomonas* Agglutinin and Related Flagellar Surface Proteins in Vitro and In Situ

URSULA W. GOODENOUGH, W. STEVEN ADAIR, PATRICIA COLLIN-OSDOBY, and JOHN E. HEUSER

Departments of Biology and Cell Biology/Physiology, Washington University, St. Louis, Missouri 63130

ABSTRACT Using the quick-freeze, deep-etch technique, we compare the structure of the cane-shaped *plus* and *minus* sexual agglutinin molecules purified from gametes of *Chlamydomonas reinhardi*. We also describe the structure of three additional gamete-specific fibrillar molecules, called short canes, loops, and crescents, which are structurally related to the agglutinins. Four non-agglutinating mutant strains are found to produce the three latter fibrils but not canes, supporting our identification of the cane-shaped molecule as the agglutinin. The heads of the *plus* and *minus* canes are shown to differ in morphology. Moreover, two treatments that inactivate the *plus* agglutinin in vitro—thermolysin digestion and disulfide reduction/alkylation—bring about detectable structural changes only in the head domain of the cane, suggesting that the head may play an indispensable role in affecting gametic recognition/adhesion. We also present quick-freeze, deep-etch images of the flagellar surfaces of gametic, vegetative, and mutant cells of *Chlamydomonas reinhardi*. The gametic flagella are shown to carry the canes, short canes, loops, and crescents present in in vitro preparations. The cane and crescent proteins self-associate on the flagellar surface into stout fibers of uniform caliber, and they align along the longitudinal axis of the flagellum. The short canes and loops co-purify with flagella but, in the presence of mica, dissociate so that they lie to the sides of the flagella. The agglutinin canes of both mating types are oriented with their hooks at the membrane surface and their heads directed outward, where they are positioned to participate in the initial events of sexual agglutination.

The first cell-cell recognition mechanisms developed by eukaryotes were probably used in fertilization. It follows that the modern sexual protozoa, although clearly “highly evolved” in their own right, may offer clues as to what kinds of cell surface molecules were originally used to mediate gametic fusion with the appropriate partner. In the unicellular alga *Chlamydomonas reinhardi*, the key sexual recognition molecule has been shown to be a large hydroxyproline-rich fibrous glycoprotein (1, 2). Since similar proteins appear to function in the organization of the extracellular matrix in higher plants (3), and since the collagens, also rich in hydroxylated amino acids, are widely implicated in organizing the tissues of the metazoa (4), an understanding of the *Chlamydomonas* agglutinin structure may yield evolutionary insights into the origins of cell-cell interactions in eukaryotes.

This paper first presents a detailed analysis of the purified agglutinin protein using the quick-freeze, deep-etch techniques developed by Heuser (5, 6). We compare the structure

of the mating-type *plus* (mt^+) and mating-type *minus* (mt^-) proteins, and describe alterations in their structure induced by proteolytic digestion and disulfide reduction/alkylation. In the course of this study we have encountered a family of proteins that are structurally related to the active agglutinin but are devoid of adhesive activity, and we report that four non-agglutinating mutant strains can produce these inactive proteins but not the active agglutinin. We then present quick-freeze, deep-etch images which show how these molecules are displayed on the flagellar surface and on the surface of flagellar membrane vesicles.

MATERIALS AND METHODS

The wild-type strains CC-620 (mt^+) and CC-621 (mt^-) and the mutant strains *imp-2* (CC-463), *imp-5* (CC-469), *imp-8* (CC-475), *imp-10* (CC-1147), and *imp-12* (CC-1149) (all available from the *Chlamydomonas* Genetics Center, Department of Botany, Duke University, Durham, NC 27706) were harvested as

plate gametes (7) and washed several times in N-free medium (7) before use. Wild-type *mt*⁺ vegetative cells were grown in liquid Tris-acetate-phosphate (8) medium to mid-log phase.

Agglutinin and agglutinin-related proteins were stripped from the flagellar surfaces of living cells with 5 mM EDTA as described in references 1 and 9. Protein purification was achieved either by Sepharose 6B/Fractogel F75 chromatography as previously described (1) or by MonoQ (Pharmacia Fine Chemicals, Piscataway, NJ) anion exchange high performance liquid chromatography using a Micromeritics system (for details see reference 10). Thermolysin (Sigma Chemical Co., St. Louis, MO) digestion was conducted by suspending purified *mt*⁺ agglutinin in 0.01 M Tris-HCl, pH 8.0, 0.01 M CaCl₂ containing 50 µg/ml thermolysin and incubating the suspension at 40°C for 2 h (11) prior to quick-freezing. Controls were incubated under identical conditions without enzyme and retained input activity. For reduction/alkylation, purified *mt*⁺ agglutinin was either treated (a) with 120 mM β-mercaptoethanol (Sigma Chemical Co.) and then with 100 mM iodoacetamide (Sigma Chemical Co.) as described in reference 10 and in the text, or (b) with 100 mM β-mercaptoethanol in 100 mM potassium phosphate buffer, pH 7.4, 100 mM KCl, 5 mM EDTA (4°C, overnight), followed by 12.5 mM dithiothreitol (Sigma Chemical Co.) (2 h, 37°C) and then 50 mM bimane (monobromotrimethylammoniumbimane) (Calbiochem-Behring Corp., La Jolla, CA) (4°C, overnight). Controls incubated for comparable periods without reducing agent and then treated with alkylating agent retained input activity. The quick-freeze, deep-etch technique was used on macromolecules as described in reference 6 except that the angle of platinum shadowing was reduced to 10°. Protein measurements were made on seven different purified preparations of *plus* agglutinin and four purified preparations of *minus* agglutinin using a Wild APT-1 stereo map reader interfaced with zoom optics, a camera lucida attachment, and a Zeiss MOP-3 digitizing tablet/computer system programmed to calculate lengths and areas. Measurements are given as the mean ± SD. To estimate the degree of accuracy achievable with this system, the same *plus* agglutinin molecule was measured 14 times. The lengths ranged from 222 to 230 nm, with a mean ± SD of 227 ± 3 nm.

Flagella were amputated from cells by pH shock (12) in 10 mM PIPES, pH 7, 5% sucrose. After pelleting most cells, the flagellar suspension (~30 ml) was underlain with 5 ml of a 25% sucrose solution and centrifuged at 2,600 g for 4 min in a swinging bucket rotor to pellet remaining cells. The supernatant overlying the pad was carefully pipetted off, avoiding the sucrose pad, and then centrifuged at 12,000 g for 5 min in a fixed-angle rotor. After removing most of the supernatant, the tube was agitated by flicks of the finger and swirling; this caused any contaminating cell walls, which form a loose pellet over the tight flagellar pellet, to go into suspension, and the suspension was pipetted off. The flagellar pellet was then suspended in fresh PIPES/5% sucrose and examined by phase-contrast microscopy. If visible cell wall contamination persisted, the centrifugation/flicking procedure was repeated until the contamination was eliminated.

Living cells were quick-frozen (5) in N-free medium. To visualize isolated flagellar surfaces adsorbed to mica, it is necessary to both remove the sucrose and increase the ionic strength of the buffer. Therefore, just before freezing, the flagella were pelleted at 12,000 g for 5 min, resuspended in 1.5 ml of KHMgE (70 mM KCl, 30 mM HEPES, pH 7.4, 5 mM MgSO₄, 3 mM EGTA), plus 10 µM taxol to minimize microtubule depolymerization, pelleted in this buffer, and frozen as a pellet mixed with freshly cleaved mica flakes (6). Although removal of sucrose causes the axoneme to curve so that isolated flagella adopt a disc shape (13), this tendency is minimized at the higher ionic strength, and most of the flagella were straight at the time of freezing. The high ionic strength is also essential for adsorption to mica, and it has no apparent adverse effect on the adhesive activity of the isolated flagella when tested against living gametes.

We should note here that the flagella of *Chlamydomonas reinhardi*, even at high ionic strength, fastidiously avoid mica surfaces, possibly as an adaptation to their natural soil environment. Adherence is improved when the mica is pretreated with polylysine, but the fibers of interest tend to sink into the polylysine so that their structure is obscured; moreover, the polylysine induces flagellar membrane lysis so that the mica becomes contaminated with tubulin and other axonemal proteins. Therefore, the *in situ* images presented here were obtained by brute-force scanning of numerous replicas, most of which contained only naked mica surfaces.

RESULTS

Structural Domains of the Plus Agglutinin

The overall structure of the purified *mt*⁺ agglutinin has been described in two previous publications from these laboratories (1, 2). For the present study we have made careful

measurements of its four structural domains, permitting a comparison of its topology with that of the purified *mt*⁻ agglutinin described in the next section.

THE HEAD: The head, previously designated a knob (2), is located at one end of the protein which we shall call the distal end. It ordinarily appears as a globular domain, 10.1 ± 1 nm (*n* = 34) in diameter (Fig. 1). Occasionally, however, it undergoes what we interpret to be a denaturation as it adsorbs to the mica, and the resultant distortion provides clues about its native configuration. As shown in Fig. 2, the denatured head ranges from anvil shaped (Fig. 2A) to distinctly bi-lobed (Fig. 2E), where the second lobe invariably lies under the first, closer to the mica surface, when viewed in stereo. This second lobe, moreover, can take the form of a tiny loop (Fig. 2, G and J), as though it were a fibrous domain circling back on itself. In Fig. 2F the globular domain is absent altogether, and only the loop remains.

THE SHAFT: The total length of the *plus* agglutinin is 228 ± 7 nm (*n* = 68), of which 10 nm is the head and 218 nm a fibrous shaft. The distal half of the shaft is usually very straight, although curves may be present (Fig. 1, G and H), whereas the proximal half usually carries one or two distinct bends. Fig. 3A plots the position of these bends along the length of the shaft. They occur at two distinct loci, one ~60% from the distal end and the other ~70% from the distal end. In Fig. 1B, for example, the protein on the right displays a 70% bend, whereas that on the left undergoes both a 60% and a 70% bend. Bends at the 70% position are the more commonly encountered, and they vary from slight flexions to sharp acute angles (Fig. 1, B, G, and H); the bends at the ~60% position, by contrast, are usually less severe. Thus, we can characterize the shaft overall as having two morphological domains: a distal inflexible half and a proximal flexible half.

The shaft measures ~6 nm in diameter which, subtracting 1 nm on either side for platinum deposition (6), yields a true width of 4 nm. If the agglutinin polypeptide contains a high content of polyhydroxyproline II helix, in analogy with the related cell wall polypeptides (14), then each chain would have a radius of ~0.8 nm (McAllester, J., D. Barry, and G. van Holst, Washington University, unpublished computer modeling studies). The short-chain oligosaccharides reported to associate with the agglutinin (15), if nested in the helix as suggested by Lamport (3), would increase the width of the whole to only ~1.8 nm. Therefore, the sugars must either extend out farther than predicted, or else the shaft must be double stranded. We have to date failed to observe any images of the shaft unraveling into composite strands, nor is there any definitive evidence of a strandedness, or a helical pitch, to the surface topology of the protein. There occasionally appears to be a seam down the center of the shaft (Fig. 1, D and F, and Fig. 2A), but this image could well be created by an accumulation of platinum grains along the sides of the fiber.

THE HOOK: The presence of a hook at the proximal terminus of the agglutinin was noted in a previous article (2); our present replicas, prepared with a shallower replication angle, greatly improve the resolution of this domain (Figs. 1 and 2). It measures 21.4 ± 2.1 nm (*n* = 34) in length, and either extends straight out at right angles to the shaft (Figs. 1H and 2H), or else curves to form a true hook (Figs. 1 and 2). Occasional proteins fail to display a hook (e.g., Figs. 1, F and G, and 2, E and G). Since these proteins are not detectably

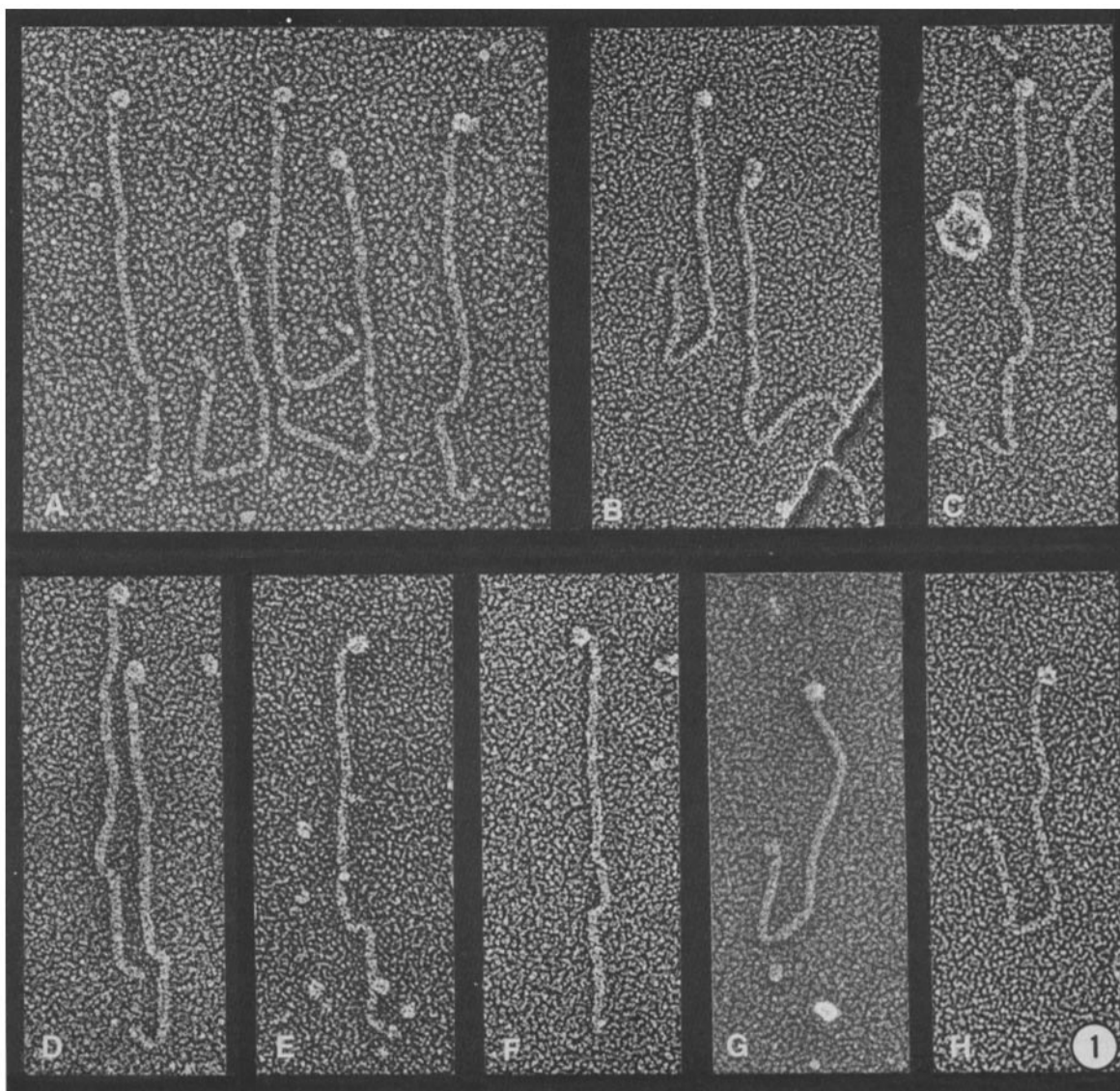


FIGURE 1 *Plus* agglutinin canes with round heads. In this and subsequent figures showing *in vitro* preparations, all proteins were column purified using the 6B/F75 system unless otherwise noted. $\times 250,000$.

shorter than their hooked counterparts, their hooks have presumably straightened out.

Structural Domains of the *Minus* Agglutinin

The biochemical properties of the purified *minus* agglutinin, detailed in a separate report (10), indicate that the *plus* and *minus* agglutinins are homologous proteins. Electron microscopy confirms this conclusion (Fig. 4), but reveals subtle differences in conformation between the *plus* and *minus* molecules.

THE HEAD: There are several differences between the *plus* and *minus* head. The *minus* head is slightly larger, measuring 11.5 ± 1.1 nm ($n = 30$) in diameter (in contrast to 10 nm), and stands considerably higher off the mica surface when viewed in stereo. Moreover, it invariably appears very round, and never assumes a bi-lobed or looped configuration (cf., Fig. 2). Therefore, the *minus* head is either less prone to denature during adsorption to mica, or else it is constructed in a different fashion from its *plus* counterpart.

THE SHAFT: The *minus* agglutinin is comparable in length (226 ± 9 nm [$n = 49$]) and width to the *plus* agglutinin,

but its shaft differs in apparent flexibility. Some 20% of the proteins on mica have fully straight shafts (Fig. 4, *D* and *E*), which is uncommon for the *plus* molecules. Furthermore, the bends that do occur are generally found at $\sim 70\%$ from the distal end of the protein (Fig. 3*B*), with no obvious flexion point at 60%, and they tend to be gentle arcs (Fig. 4*B*, *G-I*) rather than sharp turns. Perhaps the most diagnostic difference is seen at the head/shaft junction: in the *plus* protein, the shaft usually extends straight down from the base of the head (Figs. 1 and 2), whereas in the *minus* protein, the shaft typically comes out from the side of the head and then turns down. This turn can either be abrupt or can take the form of a gentle curve, causing the distal end of the protein to resemble a shepherd's crook (Fig. 4, *B*, *C*, and *E*).

THE HOOK: No obvious morphological differences distinguish the hooks of the *minus* agglutinins from those of the *plus*.

Short Canes, Loops, and Crescents

The full-length (~ 225 -nm) proteins described above invariably co-purify with adhesive activity, regardless of the puri-

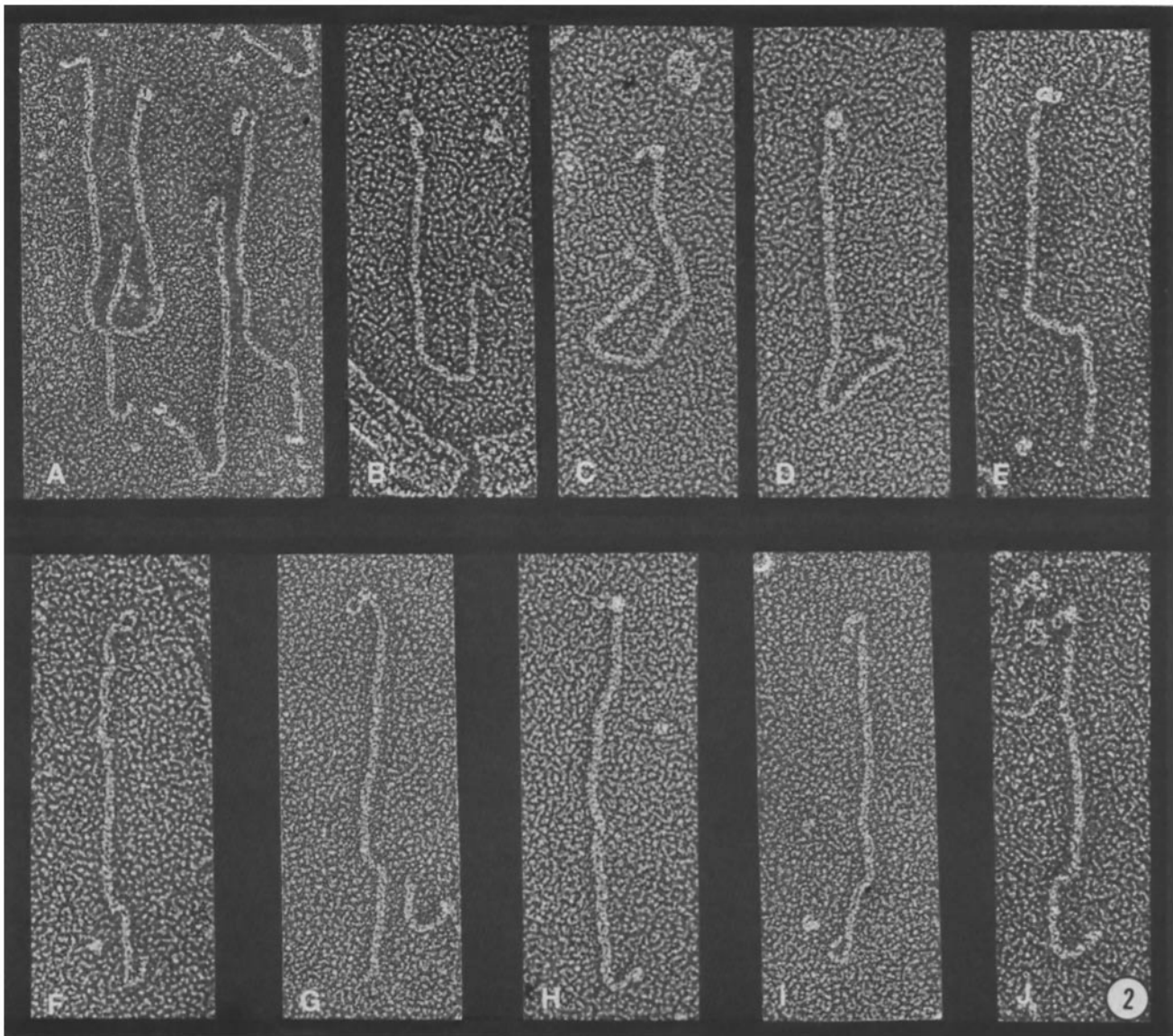
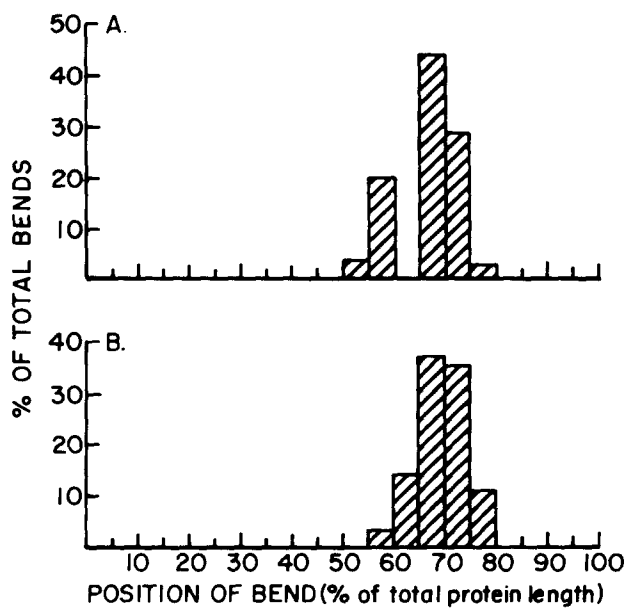


FIGURE 2 *Plus* agglutinin canes with bilobed (upper) or loop-containing (lower) heads. $\times 250,000$.



fication method used (e.g., gel filtration or anion exchange chromatography). These full-size molecules are designated canes, to distinguish them from three additional species of proteins present in both *plus* and *minus* preparations which we designate as short canes, loops, and crescents.

Representative images of these proteins are shown in Figs. 5 and 6. Their shafts are sufficiently similar to the agglutinin canes to suggest that all belong to a homologous family of proteins. We first describe their morphology and then their biochemical properties.

MORPHOLOGY: The structure of a short cane (Fig. 5) is superficially similar to the distal portion of a full-length cane in that it carries a globular, ~ 10 -nm head at the distal end of a straight shaft. However, each shaft is only $\sim 55\%$ the length of a full cane (128 ± 10 nm [$n = 78$] for *plus*, and 118 ± 11 nm [$n = 85$] for *minus*). The short cane usually also carries a

FIGURE 3 Position of bends along the shaft of *plus* (A) and *minus* (B) agglutinins, plotted as percent of total length of each molecule. Total number of molecules measured: 70 *plus*, 46 *minus*.

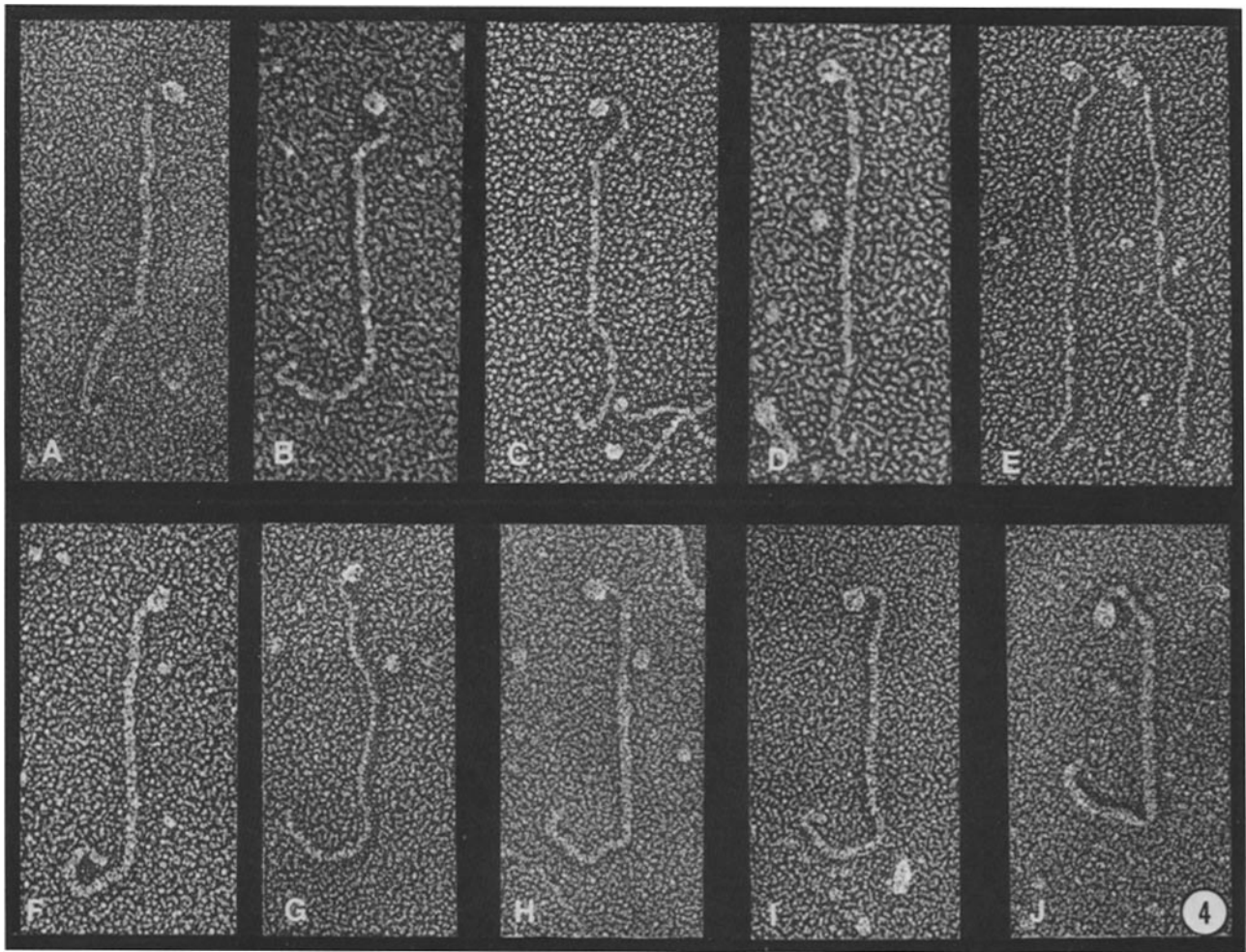


FIGURE 4 *Minus* agglutinin canes. $\times 250,000$.

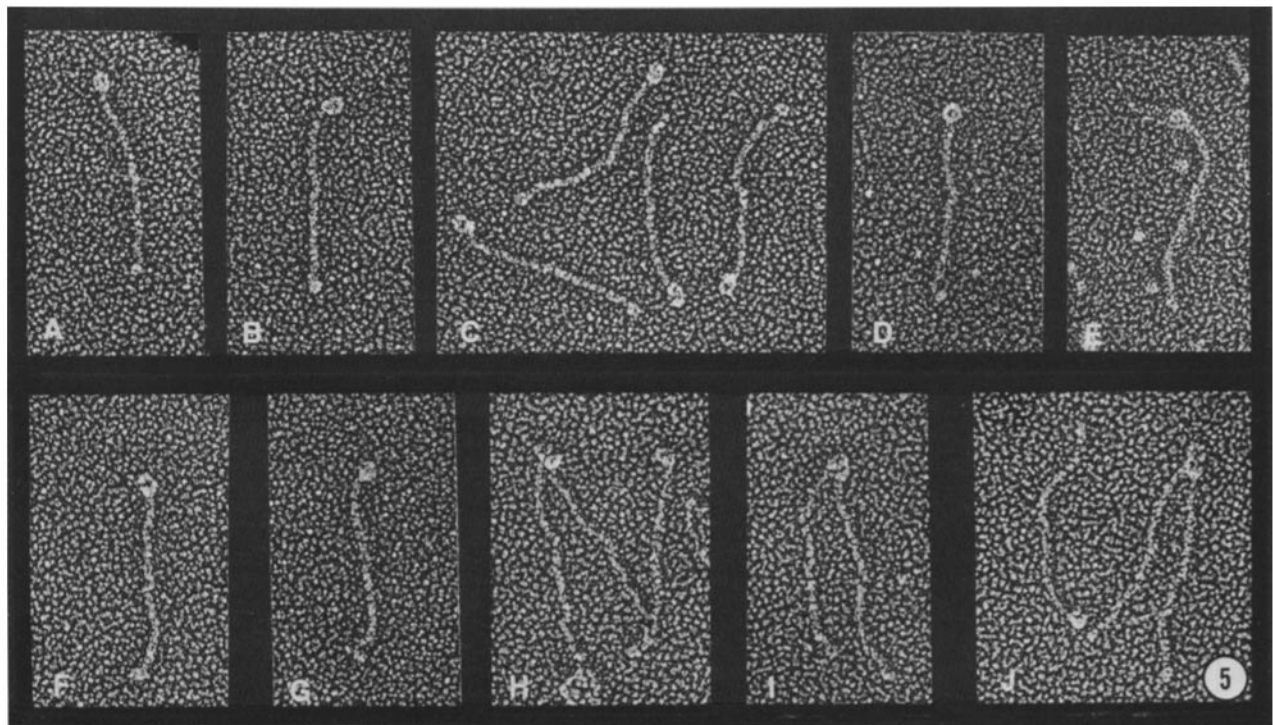


FIGURE 5 Short canes from *minus* (A-D, F, and G) and *plus* (E, and H-J) gametes. $\times 250,000$.

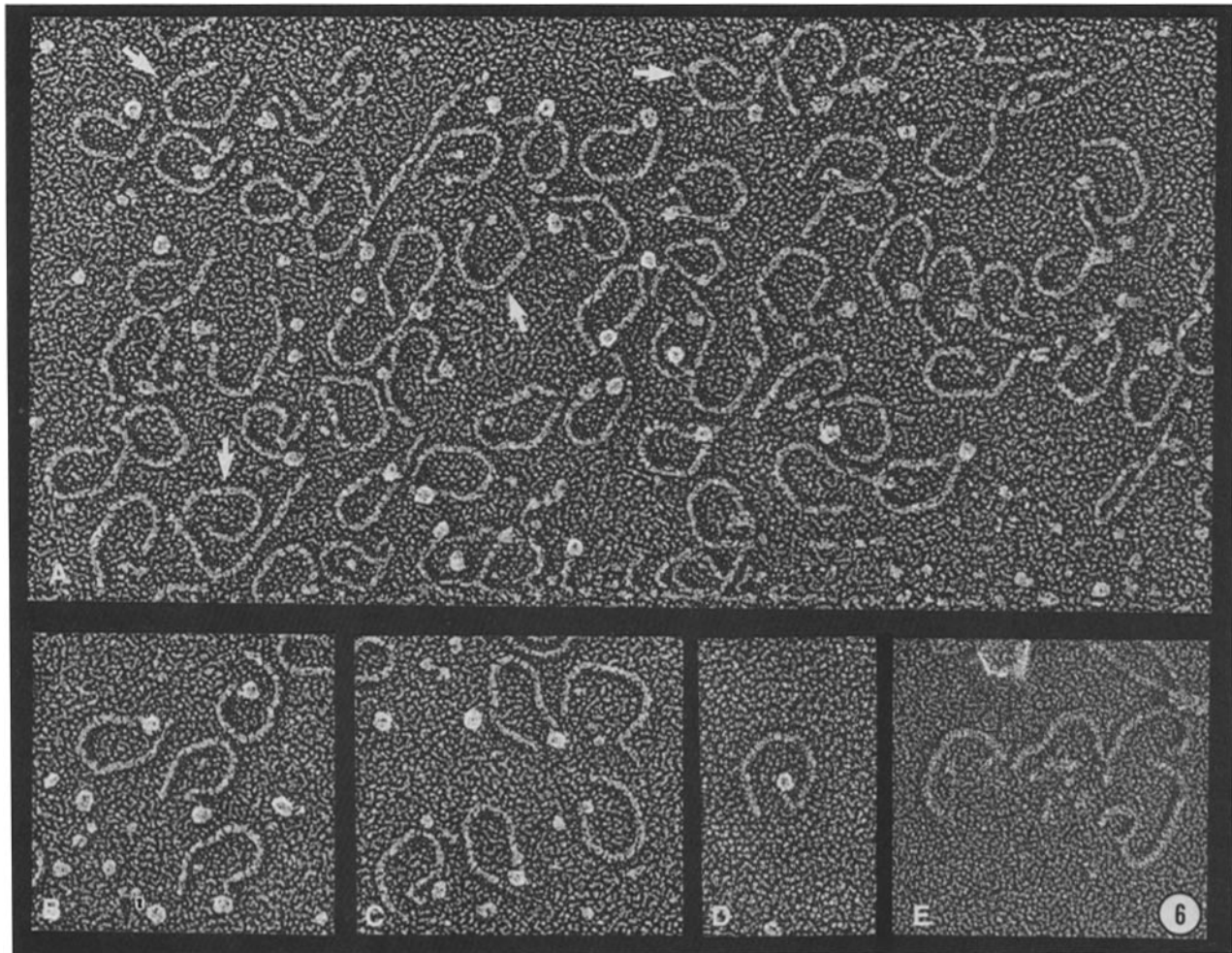


FIGURE 6 Loops and crescents. In A, crescents are indicated by arrows; the rest are loops. B–D, loops. E, crescents. A, B, and E are from the nonretained flow-through of a MonoQ column. $\times 250,000$.

small knob at its proximal end, and often associates with other short canes, either *via* its knob or its head, to form small aggregates (Fig. 5, H–J). Significantly, the head of the *plus* short cane is never observed to denature into a distinctly bilobed or anvil-shaped unit, whereas such configurations are often adopted by the heads of *plus* full canes (Fig. 2). For this and other reasons (see Discussion), we believe that the short canes are distinct biochemical entities and not proteolytic fragments of full canes.

Loops (Fig. 6, A–D) are circular fibrils that carry a prominent round head, ~ 10 nm in diameter, at one end. About 20 nm beyond the head/shaft junction, the shaft usually makes a distinct kink, seen to advantage in Fig. 6D. It then arcs to form a loop, and either terminates as a free end near the head or else makes direct contact with the head to close the circle. The total length of the loop measures 129 ± 5 nm ($n = 41$) for *plus*, and 134 ± 16 nm ($n = 67$) for *minus*; the large variation in the *minus* length is possibly of interest. The distinctive kink near the head/shaft junction, we should note, is not observed in the short canes, nor is the terminal knob of the short cane observed at the terminus of the loop; these differences discourage speculation that the loops are simply short canes that have for some reason adopted a circular configuration on the mica surface.

Crescents are also curved fibers, but they lack the heads

and the kinks that are found on the loops and are less likely to circle back on themselves to form a closed loop. Four crescents are indicated by arrows in Fig. 6A, and although it could be argued that these are simply loops that have lost their heads and fail to display a kink, the crescents as a class are distinctly shorter than loops (86 ± 7 nm [$n = 43$] for *plus*, 110 ± 10 nm [$n = 67$] for *minus*). Moreover, they tend to associate with one another to form chains (Fig. 6E). A key distinction between loops and crescents is that whereas loops are frequently encountered in EDTA extracts, indicating a relatively labile association with the flagellar membrane, crescents are rarely encountered in extracts but are abundantly associated with flagellar preparations. Much of our information about crescents is therefore presented in later sections dealing with membrane-bound fibers.

BIOCHEMICAL PROPERTIES: Crude EDTA extracts of *Chlamydomonas* gametes contain substantial levels of short canes and loops, some crescents, and agglutinin canes and wall proteins. Whereas it is relatively straightforward to rid the preparation of most contaminating wall proteins by column chromatography (1), the behavior of the short canes and loops is more erratic: in some preparations they co-fractionate with the agglutinin canes, while in others they chromatograph in different fractions (we have as yet no explanation for this variability). Invariably, however, fractions with significant

levels of short canes and loops, as judged by electron microscopy, are found to contain one or more periodic acid-Schiff-positive bands which migrate ahead of the agglutinin band in the 3% stacking gel of our SDS PAGE system. Since these bands migrate quite close to one another and often appear as a smear, we have had no success in correlating individual bands with individual fiber types. Therefore, we will designate this family of bands as B, to contrast them with the agglutinin band A (1, 10).

Fig. 7 shows four samples from anion exchange high performance liquid chromatography fractionation of an *mt*⁺ EDTA extract. Fraction 24 contains primarily the agglutinin

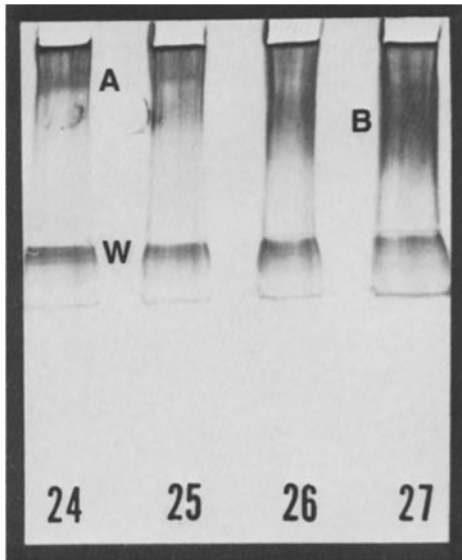


FIGURE 7 SDS PAGE of MonoQ column fractions of a *plus* EDTA extract. Peak agglutinin activity resided in fraction 24, which contains peak amounts of polypeptide A as well as a wall contaminant (W) present in all the fractions. Most of the polypeptide B material elutes from the column at higher ionic strength and is abundant in fraction 27. SDS PAGE as described in reference 1, with a 3% stacking gel and a 5-15% running gel; periodic acid-Schiff stain. Equal volumes from each column fraction were desalted, lyophilized, and solubilized in equal volumes of lysis buffer. The top of the running gel is just above the band marked W.

band A, plus a cell wall contaminant (W), and by electron microscopy it was found to contain 83% long canes and 17% short canes ($n = 105$). By contrast, fraction 27, which has little polypeptide A but large amounts of B material, contained 6% long canes and 92% short canes ($n = 191$). Loops and crescents were not present in either fraction; instead, they were located in the nonretained (flow-through) fractions of the column, which also contained considerable amounts of B material by SDS PAGE (not shown). Therefore, the circular fibers appear to carry a different net charge from the straight fibers.

Using our bioassay for *mt*-specific adhesive activity (9), activity is found only in fractions containing significant levels of polypeptide A and significant numbers of full canes. Thus in the experiment described above, fraction 24 possessed high levels of activity, whereas the nonretained fractions and fraction 27 were without activity. (As discussed in reference 9, fractions with only low amounts of agglutinin by gel analysis fail to display activity in our bioassay.) Therefore, despite their structural similarities to the cane proteins, the short canes, loops, and crescents do not appear to possess adhesive properties.

Thermolysin Degradation of *Plus* Agglutinin

We have recently shown that thermolysin digestion completely inactivates the adhesive activity of purified *plus* and *minus* agglutinins coupled to agarose beads (10, 11). We therefore asked whether incubation of the *plus* protein in thermolysin (50 $\mu\text{g}/\text{ml}$, 2 h) had any detectable morphological effect. The length and overall configuration of the digested proteins proved to be indistinguishable from the controls, but many of their heads were abnormal. Most commonly, the globular shape is replaced by a ragged, ill-defined domain (Fig. 8, A and F, arrows). In some cases, the globular conformation is absent and the distal end of the protein carries only a tiny loop (Fig. 8, C-E, arrows), which resembles the loop occasionally visualized in the untreated protein (Fig. 2, F-J). Least often, the distal end carries neither a globular head nor a loop—it is apparently decapitated (Fig. 8, B and G).

It should be noted that whereas no adhesive activity remained after thermolysin digestion of these samples, only

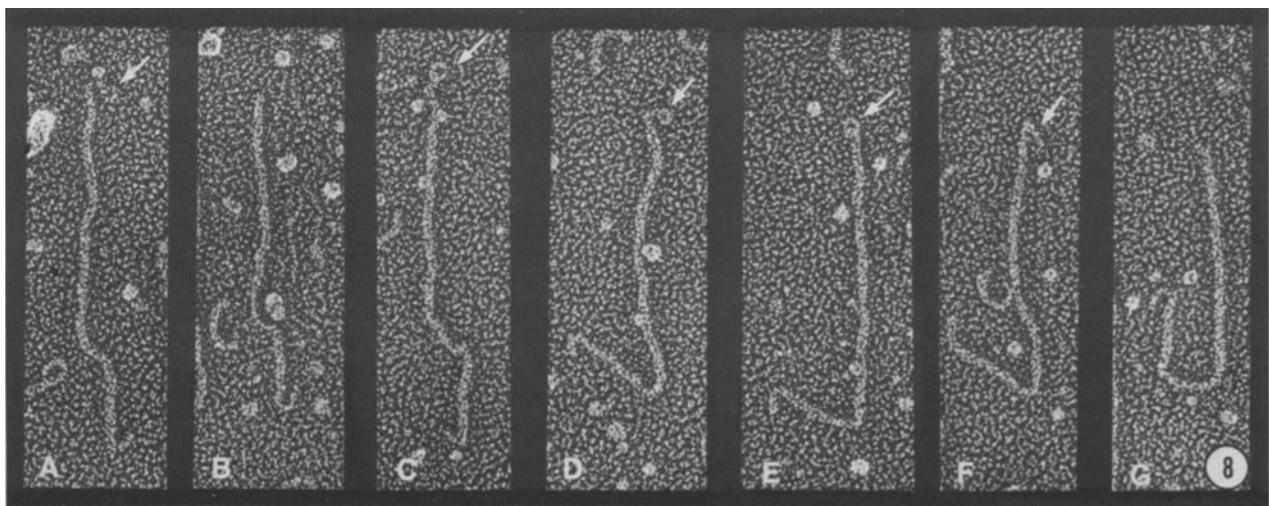


FIGURE 8 Thermolysin-treated *plus* agglutinin. Arrows indicate remains of the head region, which may resemble a small loop. $\times 250,000$.

51% ($n = 136$) of the proteins had visibly abnormal heads. One interpretation of this statistic is that inactivation is the consequence of some lesion that is morphologically undetectable, and that the “head effect” is irrelevant. The alternative possibility, which we consider more likely, is that the heads that look normal are actually in an incorrect configuration for biological activity, but that only about half of these clipped heads have proceeded to denature into visibly abnormal forms.

Reduction/Alkylation of Plus Agglutinin

Another effective way to destroy agglutinin activity is by disulfide reduction and alkylation (10, 11). When reduction is effected with β -mercaptoethanol (120 mM, 1 h, [room temperature]) and alkylation with iodoacetamide (100 mM, 1 h), there is no detectable effect on the morphology of the *plus* agglutinin (not shown), even though inactivation is complete. By contrast, when *plus* agglutinin was reduced with β -mercaptoethanol, then with dithiothreitol, and then alkylated with bismane, the resultant inactive proteins all had the structure shown in Fig. 9: the heads are uniformly absent. We have not yet ascertained why the two protocols yield such different results, but they indicate that whereas activity can be abolished without a morphological effect, one target of the reducing agents is likely to be the head.

Many of the reduced/alkylated agglutinins display a small hook at the distal end which formerly carried the head (Fig. 9, *A, B, D, and F*, arrows). This hook might be an “unrolled head”—that is, the head may be a domain of the shaft that adopts a globular configuration via disulfide linkages. Alternatively, the hook might represent the site on the shaft with which a globular head normally associates, corresponding perhaps to the looped domain sometimes visible when the head is partially denatured (Fig. 2*F*). The length of the reduced agglutinins is 229 ± 10 nm ($n = 21$), which is comparable to the normal cane length (228 ± 7 nm), with the standard deviations being too large to permit a choice between the “unrolled” and the “decapitated” models.

Mutant Proteins

Six *plus* mutants and two *minus* mutants have been isolated that lack agglutinin activity; all are either linked to the *mt* locus or controlled by *mt* (16–18). We have previously shown

biochemically that four of the *plus* mutants lack polypeptide A, but that varying levels of polypeptide B are present in the column fractions where A is expected (1). This analysis has been extended to the two *minus* mutants, *imp-10* and *imp-12*, and they also produce only polypeptides migrating in the B position (10). Electron microscopy of *imp-5*, *imp-8*, *imp-10*, and *imp-12* EDTA extracts shows that only short canes, loops, and curves are present; no canes are found (data not shown). Further information on the mutant proteins is presented in a later section.

Overviews of the Flagellar Surface

Fig. 10 shows a *minus* gametic flagellum after quick-freezing and deep-etching. Prominent are the long ($\sim 1\text{-}\mu\text{m}$) fibrous mastigonemes (*M*) described previously (12, 19, 20), which insert into the membrane surface. Also present are membrane vesicles, most round but one tubular, which carry the same knobby surface coat as the flagellum and either bear mastigonemes or else are entrapped in the mastigonemes. These presumably correspond to the membraneous vesicles that have been described as tending to bleb from flagellar surfaces (19, 20).

At higher magnification (Fig. 11), the surface coat of the gametic flagellum is seen to consist of irregular projections (*P*) which, when the membrane adsorbs to a mica surface (Fig. 12), dissociate into small units (arrows). Since the biochemical composition of the flagellar surface is dominated by a single 350-kD glycopolypeptide species (12, 19–22), each small unit may correspond to a 350-kD protein and these may aggregate on the surface to generate its rugose texture.

When gametic flagella are frozen in their low ionic-strength N-free medium rather than in the 105-mM salt solution used in Figs. 10 and 11, a very different surface topography is evident in deep-etch replicas. As shown in Fig. 13, the flagellum now carries by a dense mat of fibrous material (*F*), with the individual fibers much narrower and more numerous than mastigonemes (Fig. 10). We cannot yet explain why the system tends to collapse at the higher ionic strength.

Optimal views of this fiber system are obtained after adsorbing flagella to mica flakes at high ionic strength. Figs. 14 and 15 show a *plus* and a *minus* gametic flagellum adsorbed to mica. The fibrils (*F*) associated with their surfaces are readily visualized. Individual fibrillar types will be considered

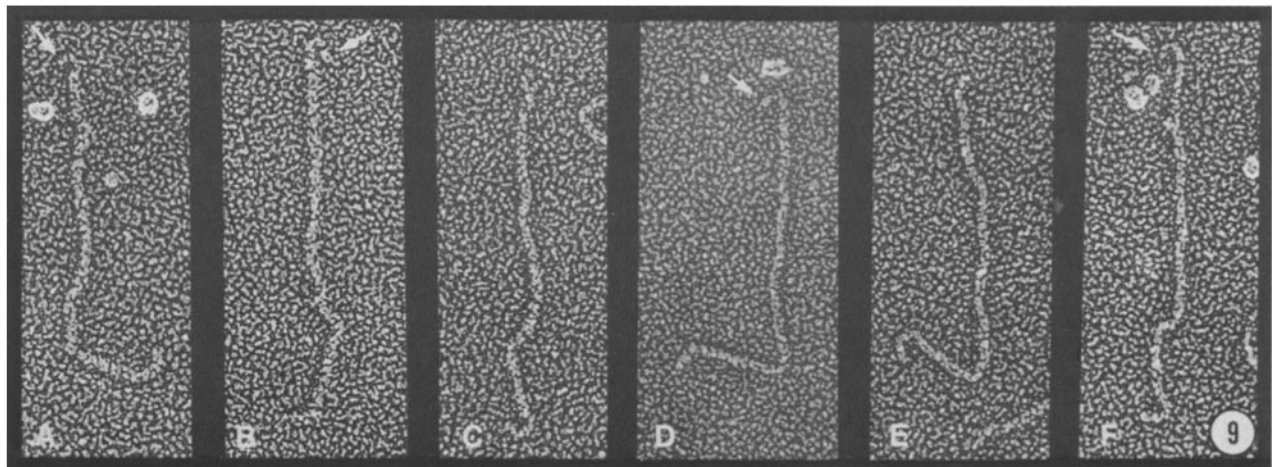
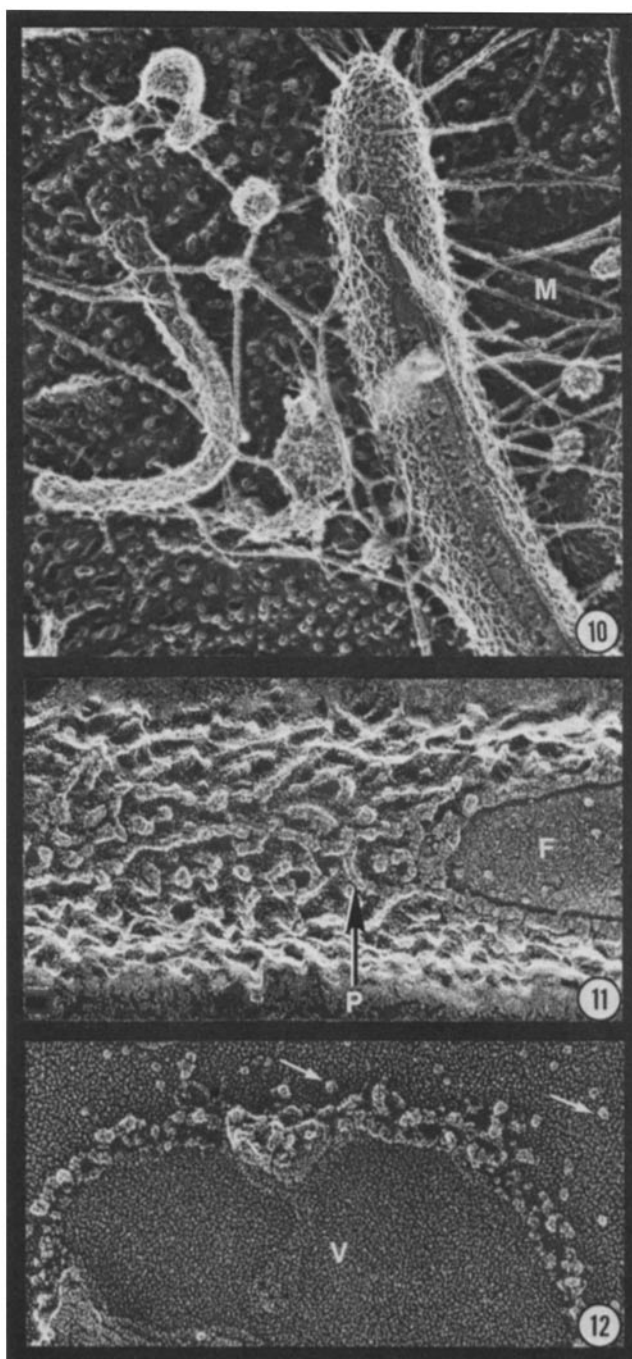


FIGURE 9 Reduced and alkylated *plus* agglutinin. Arrows indicate a curved region of the shaft in the former location of the head. $\times 250,000$.



FIGURES 10–12 (Fig. 10) Flagellar tip and associated membrane vesicles from an *mt*⁻ gamete. *M*, mastigonemes. $\times 62,000$. (Fig. 11) Flagellar surface from an *mt*⁻ gamete frozen in 100 mM salt. *F*, fracture *P* face through flagellar membrane; *P*, projections on the true flagellar surface. $\times 145,000$. (Fig. 12) Flagellar membrane vesicle (*V*) from an *mt*⁻ gamete, adsorbed to mica and fractured to remove its upper surface. The edge of the vesicle carries projections (cf. Fig. 11) which dissociate into smaller particles (arrows). These particles are also evident as background on the mica surface in Figs. 15, 25–27, and 31–32. $\times 190,000$.

in the following section. Here we call attention to three general features of their organization.

First, each fibril system appears to be aligned in a linear fashion along the longitudinal axis of the flagellum. Thus in Fig. 14, the fibrils that emanate from the upper side of the flagellum are similar in length; such an image would not arise

if they were radially or randomly disposed around the flagellum.

Second, there are two major classes of fibrils on the gametic flagellum. In Fig. 15, those labeled *F* on the left side of the flagellum are straight, whereas those labeled *C* on the upper right side are curved. To date, whenever we have seen two fibrillar systems on either side of a single flagellum, one is invariably straight and the other curved. These observations have led to the schematic diagrams drawn in Fig. 16, *A* and *B*. We suggest that the membrane carries at least four discrete linear arrays of fibrils, two straight and two curved. Depending on the angle at which the flagellum adsorbs to the mica and the amount of membrane fractured away, some replicas will display only one row of fibrils (Fig. 14) and others two (Fig. 15). The diagrams also illustrate an important point, namely, that the full length of the straight fibrils may not always be visible, since the overlying flagellum may mask a proximal portion of each shaft. As will become clear in subsequent sections, the diagrams are oversimplified in that there are probably more than four rows per flagellum; they are offered here to provide an overall orientation for viewing these rather difficult “whole mount” images.

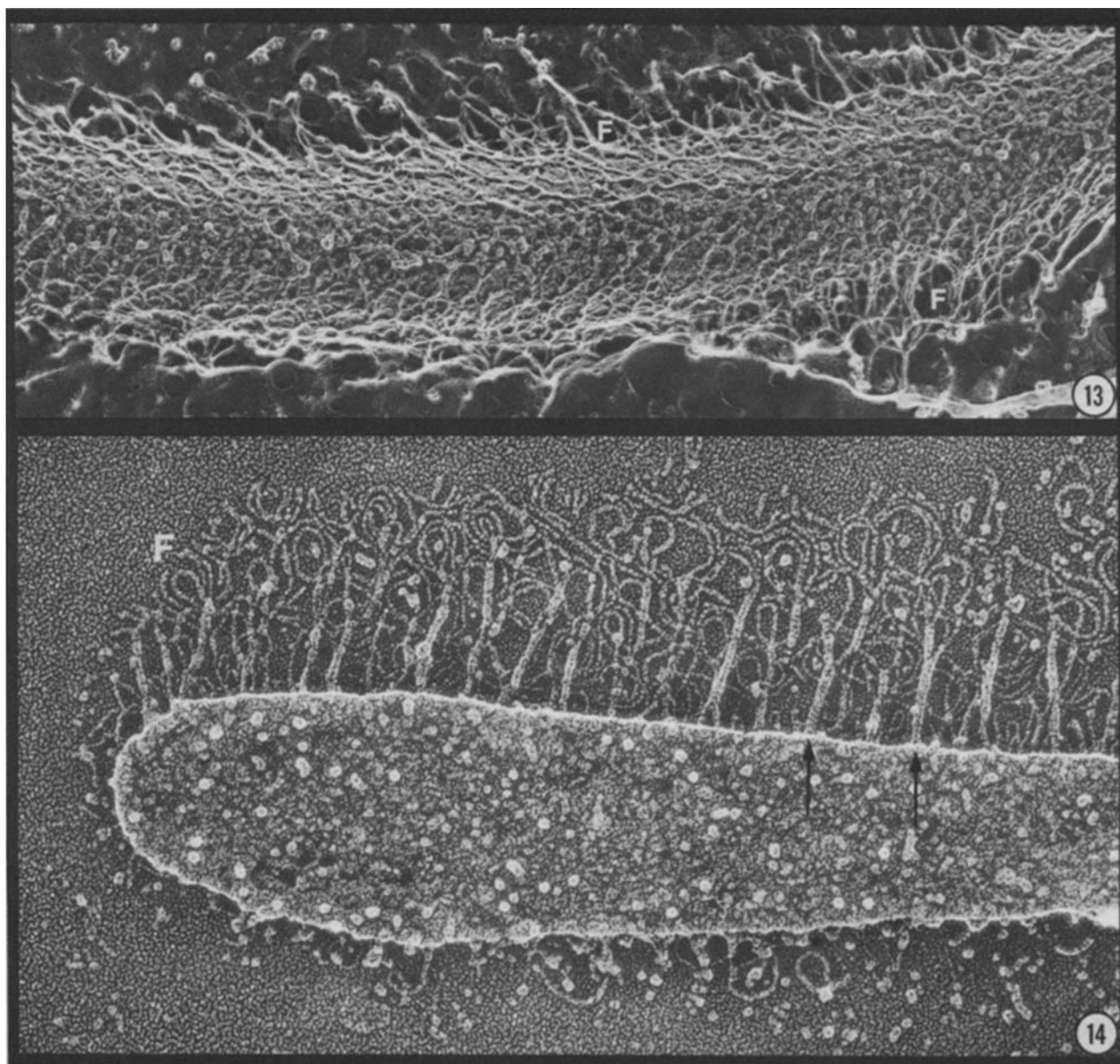
The third general feature, diagrammed in Fig. 16 *C*, is that the fibrils associate laterally to form thicker fibers. Thus in Fig. 14, the arrows point to stout fibers, spaced at regular intervals, which splay out into curved fibrils at their distal ends. We believe that these fibers are equivalent to the fibers visualized by deep-etching in Fig. 13; that is, the fibrils apparently associate into fibers *in situ*, and are induced to dissociate into their component fibrils during mica adsorption. Dissociation may be complete, as in Fig. 15, or partial, as in Fig. 14.

We can now turn to analyze the straight and curved fibrils.

Agglutinin Canes *In Situ*

The straight fibrils on the gametic flagellar surface correspond to the agglutinin canes described above. Thus the arrows on the right side of Fig. 15 point to four fibrils with ~ 11 -nm heads, curved necks, and long shafts that extend ~ 225 nm from the membrane, a morphology identical to the isolated *minus* agglutinin canes (Fig. 3). The arrowheads on the left side point to two fibrils with the same diagnostic head features, but the fibrillar lengths in this case have been foreshortened by the overlying flagellum (cf., Fig. 16 *B*). We should note that Fig. 15 represents the only instance wherein agglutinin canes have been found on both sides of the flagellum. Stereo viewing of this field shows that the flagellum was fractured at a very steep angle from right to left, and a second agglutinin row (cf., Fig. 16 *B*) was apparently included.

A more complex, but most informative, view of agglutinin disposition *in situ* is given in Fig. 17 and, at higher magnification, in Fig. 18. Shown is a mica surface to which a *minus* gametic flagellum, from a living gamete, first adsorbed and then ripped away, leaving behind a long boomerang-shaped row of membrane vesicles (two are labeled *V* in Fig. 17). A dense system of fibrils, some curved (*C*) but most straight, associates with these vesicles. Along the plane designated by the two *H*'s is an array of globular heads associated with straight fibrils that stack up in parallel, some emanating from the vesicle to the left, others free on the mica surface but presumably once associated with membrane to the right. These fibrils extend ~ 225 nm from the vesicle surface, and



FIGURES 13 and 14 (Fig. 13) Flagellar surface of an *mt*⁺ gamete frozen at low ionic strength. *F*, fibrous material. × 82,000. (Fig. 14) Flagellum of an *mt*⁺ gamete adsorbed to mica and fractured through the flagellar membrane. *F*, fibrous material associated with the membrane. Arrows, stout fibers giving rise to curved fibrils. × 173,000.

those indicated by arrowheads in Fig. 18 display the diagnostic curved neck of the *minus* agglutinin. The arrows in Fig. 18 point out three examples where agglutinin fibrils are associated at their proximal ends to form thicker fibers (Fig. 16 C).

The dense packing of agglutinin fibrils along the flagellum of *minus* gametes (Fig. 15 and 17) is also found for the *plus* flagellum, as seen on the left side of Fig. 19. In both mating types, the canes associate with the membrane via their hook ends and display their heads to the external medium.

Curved Fibrils (Crescents) In Situ

The curved fibrils on the surface of gametic flagella are sufficiently similar in morphology to the crescents found in EDTA extracts (Fig. 6 E) that we will equate the two here, although we stress that biochemical proof for this equation has not yet been obtained. The crescent system displays a

variety of configurations on the mica surface. At one extreme, as in Fig. 14, the bulk of the material is bundled into thick fibers which splay at their proximal ends into a tangle of curved fibrils. In Fig. 19, this same configuration is found at the lower right side of the field, but it is apparent that the crescents arc from one fiber to the next, forming orderly concentric tiers. Fig. 20 shows crescents that are not conjoined into fibers but instead circle back on the membrane or else contact one another. Figs. 21–23 show the other extreme, namely wide mats of crescents that anastomose with one another, forming a labyrinth which defies the identification of individual units. Since there is no evidence to the contrary, we will assume that the mats represent unraveled versions of the tiered fibers, but further study may indicate that the two are independent systems.

Figs. 24–27 show small membrane fragments (white central element) with attached crescents. The ends of the fibrils may



FIGURE 15 Flagellum from an mt^- gamete. *F*, straight fibrils; *C*, crescent fibrils; arrows and arrowheads, agglutinin canes with recognizable distal morphology; *M*, mastigoneme-bearing terminal fibril (small arrow). $\times 115,000$.

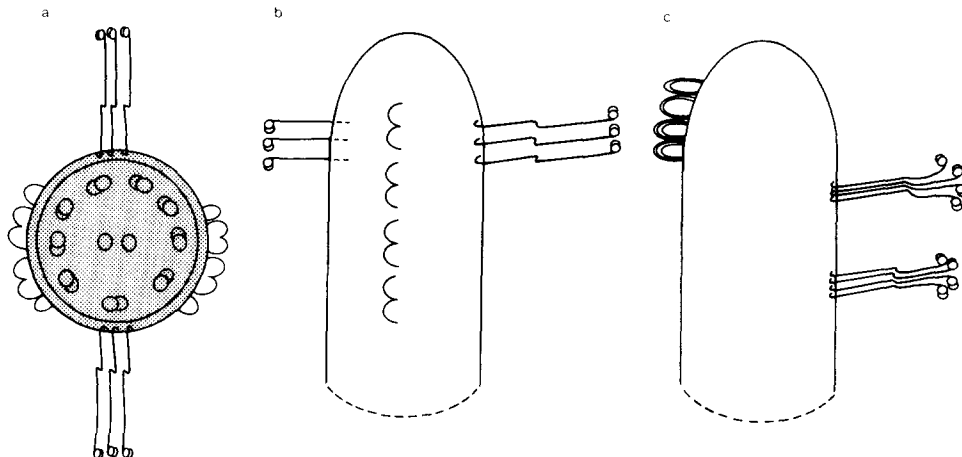
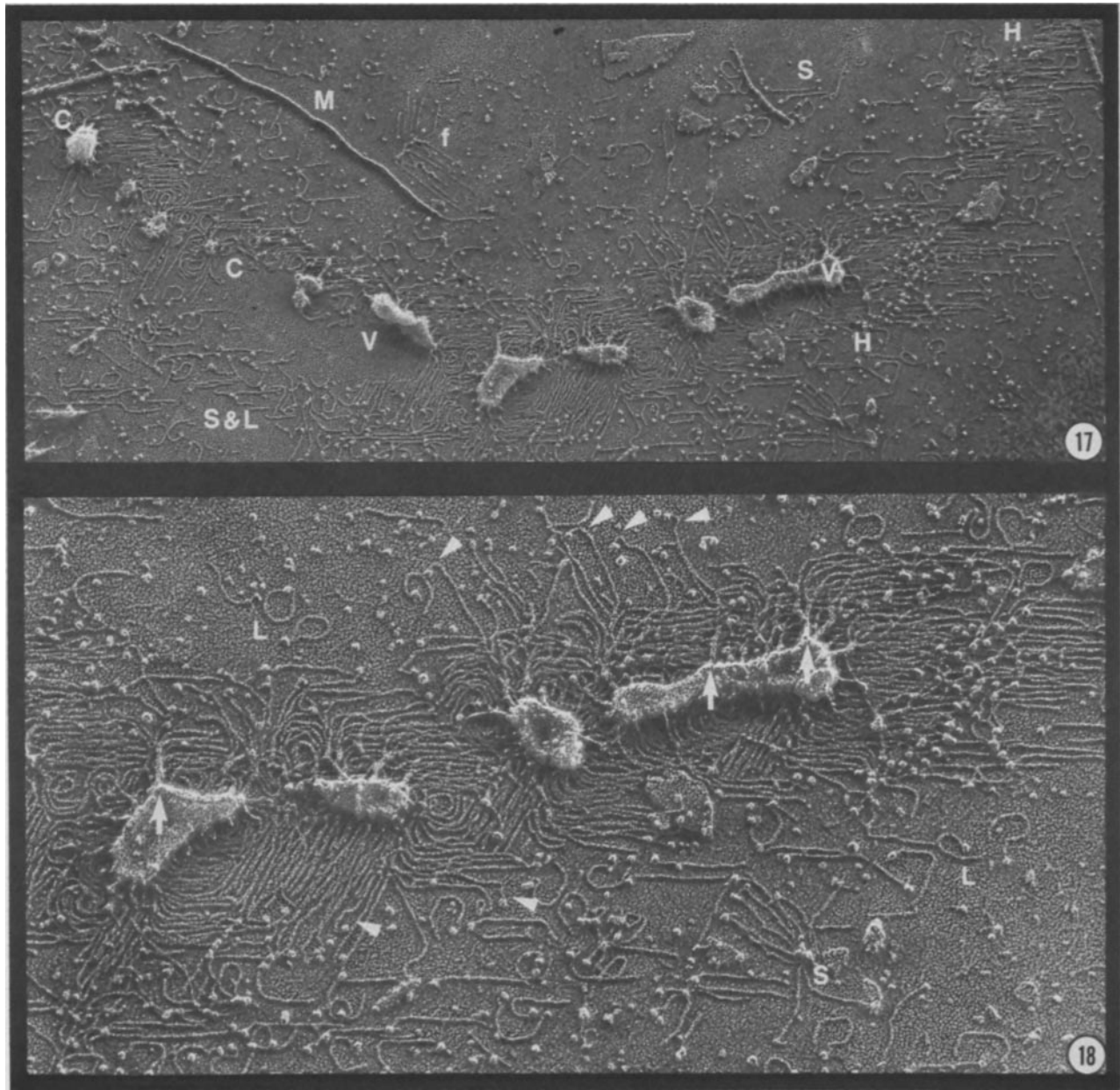


FIGURE 16 Schematic diagrams of the distribution of canes and crescents on the flagellar surface seen in cross section (A) and longitudinal section (B). C diagrams the association of these fibrils into filaments.



FIGURES 17 and 18 Survey and higher-magnification view of vesicles (V) left by a gametic mt^- flagellum that had adsorbed to mica. C, crescents; H, heads of agglutinin canes; arrowheads, canes with recognizable distal morphology; arrows, association of cane fibrils into fibers at their proximal ends; *f*, fishbone unit from a cell wall (23). $\times 68,000$ and $\times 136,000$, respectively.

associate with the membranes, with another fibril, or extend out free. In many instances (e.g., Fig. 27, arrow) the fibrils adopt a V-shape; whether these are formed by two fibrils joined at one end or by a single fibril that makes an acute bend is not clear. More generally, the ambiguous beginnings and endings of the crescents preclude any meaningful measurements of their *in situ* lengths.

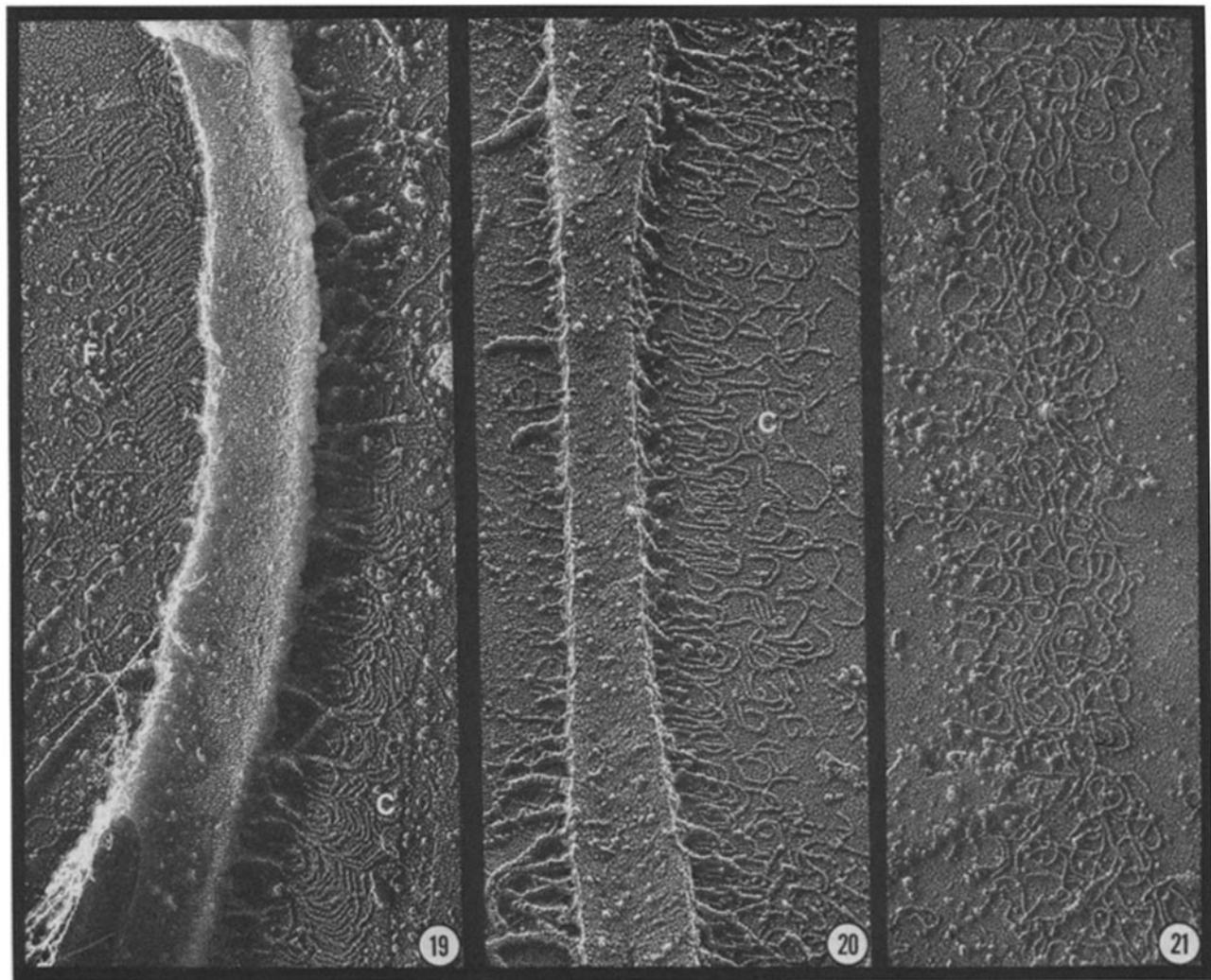
Fig. 28 (an enlargement from Fig. 17) and Fig. 29 show vesicles that carry both crescents and canes in close proximity. Such images again suggest that Fig. 16 is oversimplified in the sense that the arrays of crescents and canes may in fact be close if not contiguous, encouraging speculation that they may be functionally interrelated.

Vegetative and Mutant Flagella

Vegetative cells of *Chlamydomonas* are mitotic and lack all gametic phenotypes, notably sexual adhesiveness; therefore,

their flagella would be expected to lack any fibrillar systems important for mating. Fig. 30 shows a typical vegetative flagellum. In addition to "regular" mastigonemes (*M*), the surface carries only a sparse system of fibrils (*F*) with knobs (*k*) at their distal ends. These emanate primarily from one side of the flagellum and each is exposed by roughly the same length on a given side, suggesting, as with the gametic fibrils (Fig. 16), that they attach along a single longitudinal axis. The longest of these fibrils (Fig. 30, arrows) are at least 350 nm long, and since these have the same distal morphology as the shorter species, we believe that the latter are foreshortened by overlying membrane (cf., Fig. 16*B*). No fibers with the morphology of either canes or crescents have been observed on vegetative flagella.

A second source of non-adhesive flagella is our collection of non-agglutinating mutants, whose genetics and biochemical properties are described elsewhere (1, 10, 16–18). We have



FIGURES 19–21 Flagellar surfaces of *mt*⁺ gametes. *F*, agglutinin fibrils; *C*, crescents. The mat of crescents in Fig. 21 was contiguous to a flagellum (cf. Figs. 22 and 23). (The globular material to the extreme right in Fig. 19 is an accumulation of salt along a ridge in the mica, not globular heads.) $\times 115,000$.

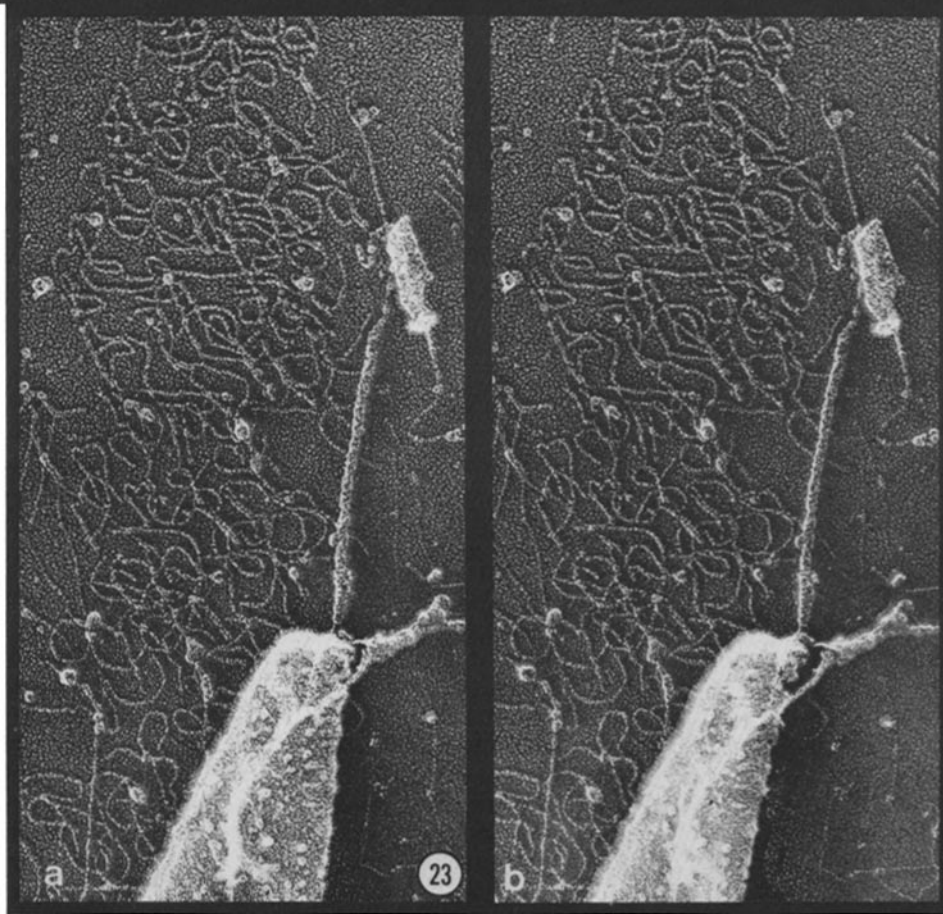
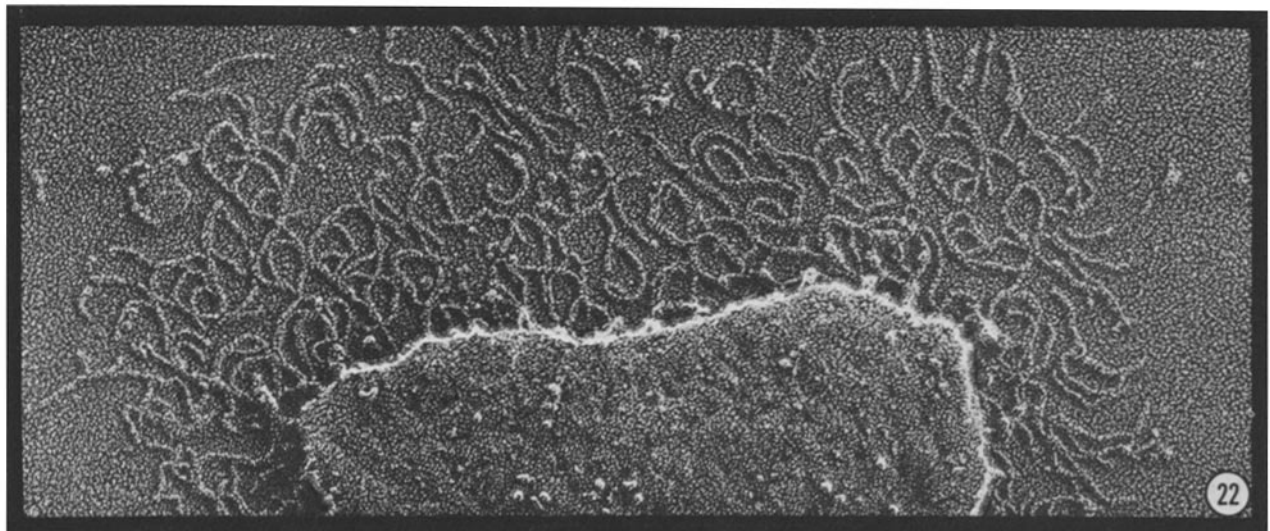
examined mutant flagella from *imp-2* and *imp-5*, which mark the *sag-1 mt*⁺ locus, *imp-8 (sag-2, mt*⁺), and *imp-10* and *imp-12 (sad-1, mt*⁻). None carries any agglutinin canes. All, however, persist in displaying a normal system of crescents: Figs. 31 and 32 illustrate, respectively, a mat array from *imp-5* and a tiered-fiber array from *imp-8*. Since these strains are non-adhesive, such images demonstrate that the crescents, at least in the absence of canes, fail to participate in agglutination.

Loops and Short Canes

In addition to the fibrils associated with the flagellar membranes, we frequently encounter, in gametic but not vegetative preparations, fibrils in the vicinity of adsorbed flagella which lie free on the mica surface. Some are straight proteins (Figs. 17 and 18, *S*) with globular heads; these are indistinguishable in length (119 ± 6 nm, $n = 33$) and in morphology from the short canes recovered from chromatographic columns (Fig. 5). Others are looped proteins (Figs. 17 and 18, *L*) with the same length (126 ± 6 nm, $n = 29$) and morphology as the loops encountered in flagellar extracts (Fig. 6). Free short canes and loops are also found in flagellar preparations from the non-agglutinating mutants (Figs. 33 and 34, *S* and *L*). In

general, free loops are more commonly encountered than free short canes and the short canes may be aggregated together (Fig. 18, *S*) as they often are in vitro (Fig. 5, *H–J*). We have yet to encounter any free long canes in our whole cell or flagellar preparations, presumably because their association with the membrane surface is stable to mica adsorption.

We assume that the short canes and loops derive from the flagella, since they are common in purified flagellar preparations which are washed several times (by contrast, they are never encountered when purified cell walls are mixed with mica flakes [23]). However, we have yet to obtain any images that demonstrate their unequivocal association with the membrane surface. This statement must quickly be qualified, since when we obtain images such as the left-hand side of Fig. 15, where straight ~ 120 -nm fibrils are emerging from a large flagellum, we cannot prove that they are obscured full-length canes and not short canes. However, we have not yet observed any examples of small vesicles bearing short canes (Figs. 24–29), and these should be easy to recognize. Since images such as Fig. 17 suggest that the short canes in the field were once attached to the flagellum that touched down on the mica, we are led to propose that the short canes associate with the



FIGURES 22 and 23 Flagellar surfaces of *mt⁻* gametes showing mats of crescent fibrils. $\times 190,000$ and $\times 150,000$ (stereo pair), respectively.

flagellar membrane surface in a fashion that is extremely unstable to the presence of mica flakes.

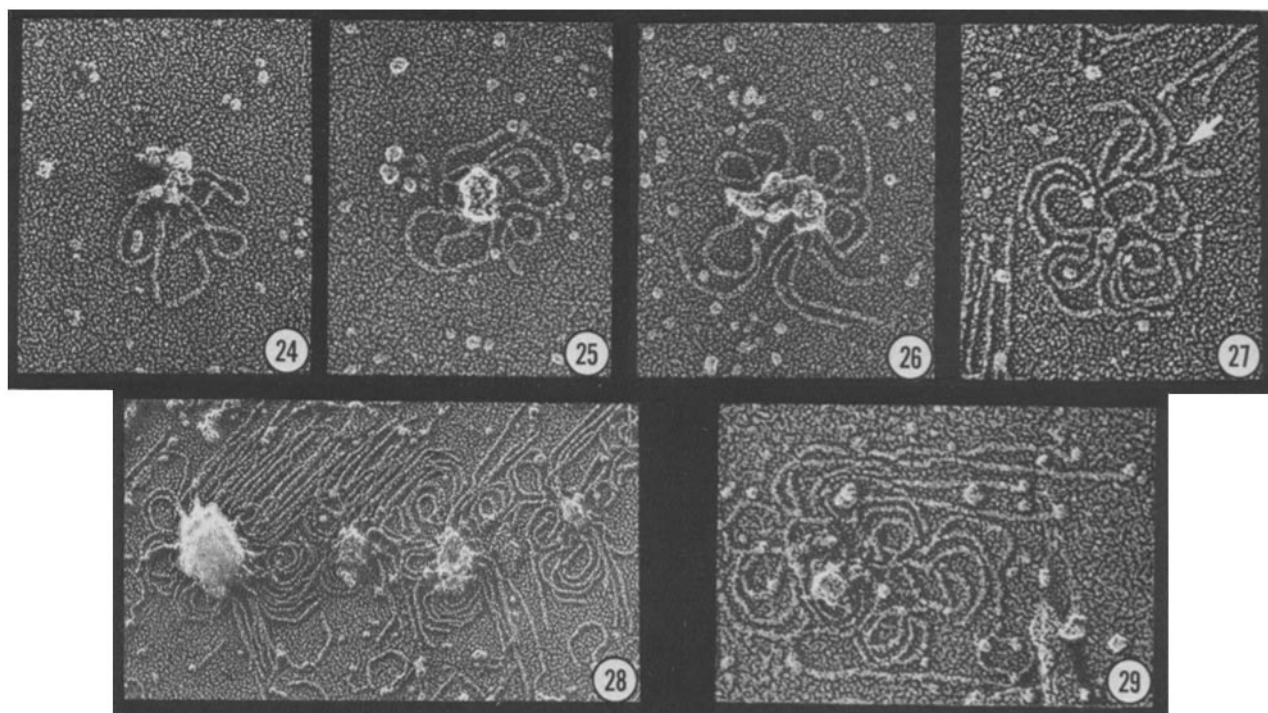
It is tempting to equate the loops with the crescent fibrils on the flagellar surface, and this possibility remains open for the curve species seen looping out from the membrane surface since we cannot visualize their membrane attachment sites. However, when we view the crescent arrays *en face* (Figs. 21–23, 31), they never display the prominent round heads that associate with the loops. Therefore, as argued above, the most

likely *in vitro* candidates for the mat-forming proteins are the crescent species.

DISCUSSION

Agglutinin Structure In Vitro

The observations presented in this paper suggest that the globular head of the agglutinin molecule is essential to its activity. Thus the head differs in size and shape in the *plus*



FIGURES 24–29 Small flagellar membrane fragments (white centers) with associated crescents (upper) or crescents plus canes (lower). All are mt^+ except Fig. 28, which is mt^- . Arrow, V-shaped configuration of crescents. All are $\times 190,000$ except Fig. 28, which is $\times 136,000$.

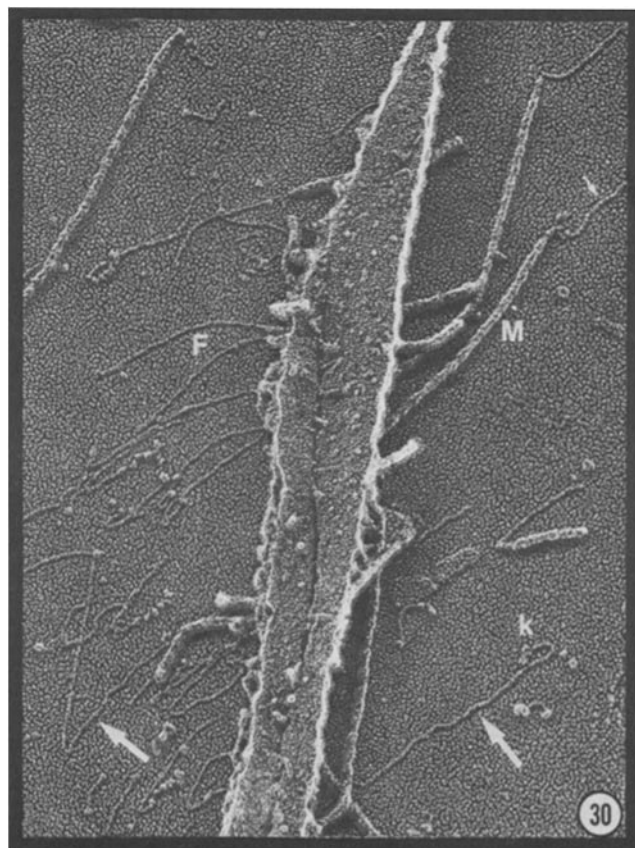


FIGURE 30 Flagellum from an mt^+ vegetative cell. *M*, mastigoneme carrying terminal fibril (small arrow) (cf. Fig. 15). A system of knobbed (*k*) fibrils is seen at *F*; large arrows indicate two long specimens. $\times 136,000$.

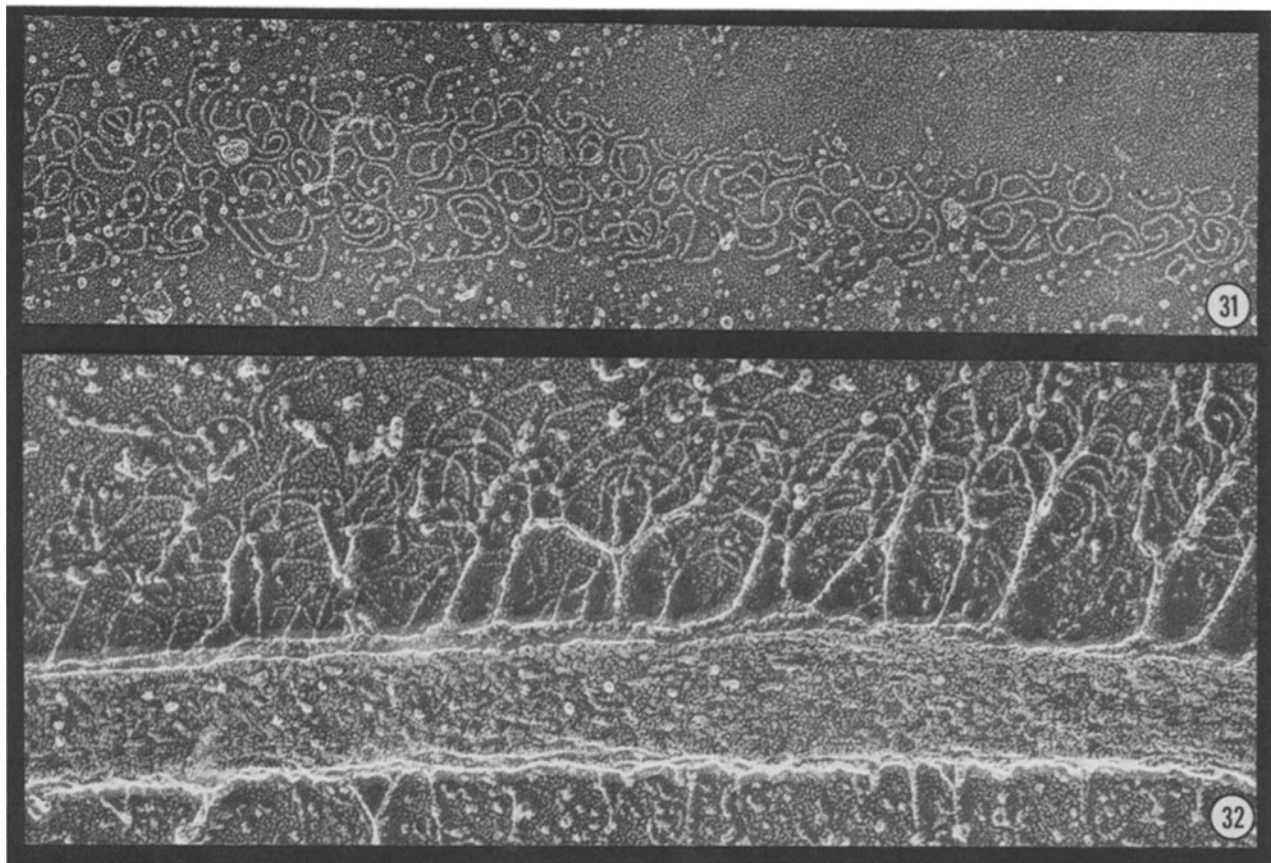
and *minus* proteins (Figs. 1–3), and two treatments (thermolysin digestion and reduction/alkylation) which abolish agglutinin activity also disrupt the morphology of the head (Figs. 8 and 9).

The shafts of the *plus* and *minus* agglutinin species are identical in length and width. However, the *minus* species appears less flexible than the *plus* and lacks one of the two distinct flexion points exhibited by the *plus* (Fig. 3). We have as yet no idea whether these differences play a role in adhesion or whether they are non-essential variations on a common structural theme. We can, however, say with considerable certainty that the two agglutinin proteins are highly homologous (see also reference 10). This finding stands in sharp contrast with the yeasts, wherein the sexual agglutinin of one mating type is a large mannoprotein and the other is a smaller species having distinctly different biochemical properties (reviewed in 24).

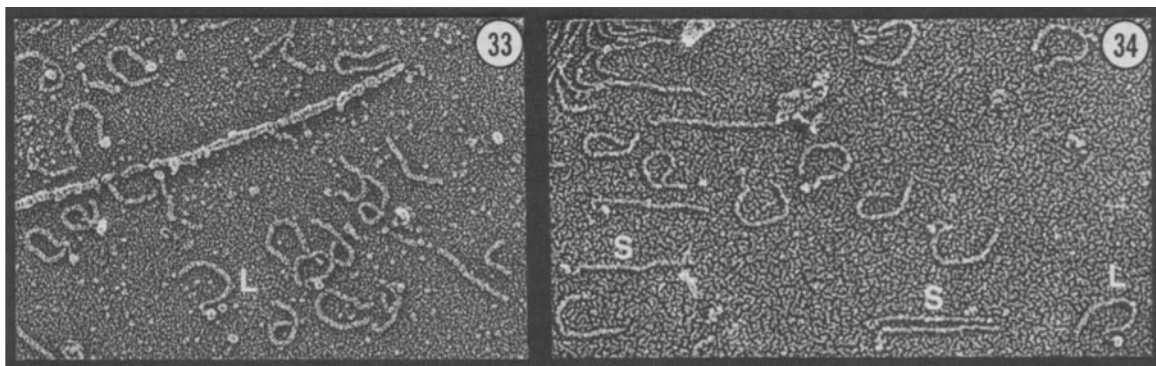
Short Canes, Loops, and Crescents In Vitro

In addition to full-length canes, EDTA extracts contain three other fibrillar species which derive from the flagellar surface, namely short canes, loops, and crescents (Figs. 5 and 6). Since these proteins are non-adhesive and have no known biological activity, we have no bioassay to monitor their individual purification. Moreover, they all migrate in a similar, poorly defined position by SDS PAGE (Fig. 7). Therefore, the only way we can distinguish them from one another at present is by electron microscopy.

The morphological similarities between the long canes and these three shorter fibrillar species leads us to conclude that they are related. In the paragraphs below we assess four possible forms that these relationships could take.



FIGURES 31 and 32 Crescent fibrils from the *imp-5* (upper, mat configuration) and *imp-8* (lower, tiered-fiber configuration) non-agglutinating mutant strains. $\times 125,000$ and $\times 188,000$, respectively.



FIGURES 33 and 34 Loops (L) and short canes (S) derived from purified flagella of *imp-5* (left) and *imp-12* (right). $\times 115,000$ and $\times 140,000$, respectively.

One possibility is that the shorter species are generated from the full cane by proteolysis. There are several reasons why this possibility appears unlikely. (a) The agglutinin cane is in general resistant to proteases (10, 11), and thermolysin, which abolishes *in vitro* activity, alters the structure of the head (Fig. 8) but fails to cut the shaft into smaller units. (b) If we imagine the full cane clipped into two halves, its straight distal half would most likely generate the short cane, and its more curved proximal half would most likely generate the loop. However, the head of the *plus* short cane fails to denature on the mica surface (Fig. 5), whereas the head of the *plus* cane often does so (Fig. 2), arguing that they are not the same entities. Moreover, the conspicuous head on the loop (Fig. 6) is absent from the proximal half of the full cane. And finally, the summed

length of the short cane (~ 120 nm) and the loop (~ 130 nm) is significantly greater than the length of the full cane (~ 225 nm). (c) Four mutant strains, mapping to three gene loci, produce the short fibers but fail to produce full-length canes. Therefore, the proteolysis hypothesis requires making the ad hoc proposition that all these mutants produce a protease which quantitatively cuts their long canes into shorter pieces.

A second possibility is that the full canes are formed by noncovalent associations between the shorter units, and that dissociation can occur during isolation/purification to generate short "monomers." By this hypothesis, the mutant strains would all produce monomers that are unable to associate into polymers. The discrepancies in length and morphology listed above when considering the proteolysis hypothesis would

apply here as well. Moreover, it is not clear why both dissociated subunits would lack adhesive activity. Finally, the hypothesis predicts that the full cane would display two bands by SDS PAGE, whereas it in fact migrates as a single band (1).

The third possibility is that the short canes and loops are biosynthetic precursors of the full canes and are covalently spliced together, with concomitant changes in length and morphology, at the flagellar surface. Fig. 35 diagrams such a sequence. The loop and the short cane are first spliced together, releasing the knob on the loop to expose the hook; the non-adhesive head contributed by the short cane is then modified to an adhesive form (additional features of the hypothesis are given in the legend to Fig. 35). The mutant strains, by this hypothesis, would be defective in splicing activity, and indeed, the generation of short canes and loops might occur by a common pathway in both *plus* and *minus* gametes, with *mt*-specific splicing events creating the mature complementary adhesions. The posttranslational processing of the yeast mating hormone, the α -factor, is effected by an *mt*-specific enzyme (25), and small collagenous polypeptides synthesized by *Caenorhabditis elegans* larvae are covalently spliced together into larger species following translation (26). Therefore, there are biological precedents for this kind of proposal, but whether it is applicable to *Chlamydomonas* remains to be tested. We are currently attempting to isolate the mRNA(s) specifying the agglutinin; once accomplished, the size(s) of the mRNA(s) should indicate whether the agglutinin is initially synthesized as two (or more) smaller proteins.

The fourth possibility is that the various fibrous polypeptides on the gametic flagellar surface, although related structurally, and presumably evolutionarily, are unrelated to one another in function. If this is the case, then the function(s) of the loops, canes, and crescents remain to be elucidated. All our biochemical, genetic, and structural data, however, reinforce our original conclusion (1) that the cane is the agglutinin of *Chlamydomonas*.

Fibrillar Proteins Occupying the Flagellar Surface

Our in situ images document that the vegetative flagellum carries a glycoproteinaceous coat assembled from globular material, fibrous mastigonemes, and a sparse population of long (~350-nm) fibrils (Fig. 30) of unknown function. The gametic flagellum retains the coat and mastigonemes and possibly also the long fibrils, but adds an abundant collection of additional fibrillar species.

The agglutinin canes are shown to attach to the membranes by their hook end and to display their head ends outward (Fig. 15, arrows), the disposition expected if, as suggested by the in vitro modification experiments, the heads mediate the initial recognition/adhesion events between *plus* and *minus* gametes. Images such as that in Fig. 17 indicate a density of ~140 agglutinin canes per μm . If we assume that a row extends from base to tip of the flagellum (~12 μm) and that there are two rows per flagellum, then we arrive at about 2.4×10^3 copies per flagellum, a larger number than that deduced previously by more indirect estimates (1).

In addition to the agglutinin canes, the gametic flagellar surface is shown to carry a system of fibrils which associate strongly with the membrane, carry no detectable heads or knobs, and abut on each other to create a labyrinth of curves which can take the form of a wide mat (Figs. 21–23, 31).

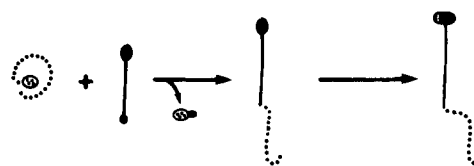


FIGURE 35 Postulated construction of agglutinin molecule: a hypothetical scheme for the generation of agglutinin canes from short canes and loops. The loops and short canes, which associate only weakly with the flagellar surface, may be secreted from the cell as soluble proteins (much like collagen precursors), associate with the flagellum via low-affinity binding sites, and may there be converted into full-length canes via this postulated splicing reaction. Since the full-length canes have a high affinity for the flagellar surface and are never found free on the mica, the splicing reaction would have to expose or create a membrane-binding domain which, in the mature protein, appears to be the terminal hook. Possibly, therefore, the 20-nm "kink" in the loop protein may be the precursor of the agglutinin hook, with its membrane-binding domain blocked by its terminal knob (stippled circle in the figure). A key event in the splicing reaction would in this case be the removal of the knob and the concomitant attachment of the hook to the flagellar membrane.

Although we have as yet no experimental data for this suggestion, the morphology of the units in these networks most closely resembles the crescent fibrils that we occasionally encounter in our EDTA extracts (Fig. 6E). The crescents are also present on non-adhesive mutant gametes but not on vegetative cells. Since the mutants are capable of sexual signaling (27), the crescents might function in this process, or they may participate in some other, gamete-specific activity yet to be defined.

Finally, our in situ images show that the short loops and canes present in EDTA extracts co-purify with isolated flagella but are released onto the mica surface during adsorption. They are gamete-specific and produced by non-agglutinating mutants, but we have no notion as to their function except to suggest that they might represent agglutinin precursors (Fig. 35).

Flagellar Surface Domains

As first pointed out to us by Dr. G. E. Palade, our images indicate that the fibrous elements of the flagellar surface are not disposed randomly but are instead confined to discrete linear avenues. That the fibrous mastigonemes are organized in two linear rows was in fact proposed by Bergman et al. (19). Here we expand this concept to include the other fibrillar surface elements, as summarized in Fig. 16.

Several biological observations might be explained by this linear disposition of surface fibrils. First, it could explain why adherent flagella in the *Chlamydomonas* mating reaction are seen to line up side by side, or at best loosely intertwined, rather than twisting around one another (13, 28–30). By postulating the presence of two rows of agglutinins on opposite sides of the flagellum, moreover, one can explain the "clumping" patterns observed in mating mixtures, wherein one flagellum can line up with at least two different flagella of opposite mating types (13, 28–30). Finally, the observation may well bear on the phenomenon known as surface translocation, described by Lewin (31) and Bloodgood (32), wherein objects such as polystyrene beads first adhere to the flagellar surface of *Chlamydomonas* and then move up and

down the flagellum along linear avenues. Although our micrographs offer no insight on the translocation mechanism per se, the linear rows of fibrils on the surfaces of vegetative flagella, and the more abundant rows on the surfaces of gametic flagella, may represent the attachment sites for these beads. Alternatively, the beads may associate with domains of the flagellar surface that are free of fibrils, the fibrils serving as "hedgerows" that restrict their movement to linear pathways. Since a variety of experimental treatments have been shown to abolish bead binding and/or translocation (33, 34), the effects of these treatments on fibrillar integrity can be put to test.

Longitudinal arrays of surface molecules require the imposition of systems that direct and anchor particular proteins to particular domains. The obvious longitudinal elements in the flagellum are the axonemal microtubules, and previous investigators have documented that electron-dense material extends from the doublets to the membrane (35) and that intramembranous particles may align along the doublets (19, 36). If each doublet can organize an array, then the flagellar surface could potentially carry nine linear domains, and the model drawn in Fig. 16 undoubtedly represents an oversimplified version of flagellar surface topography.

Association of Fibrillar Elements into Fibers

Images such as the one in Fig. 18 indicate that the shafts of the agglutinin canes associate with one another, at least at their proximal ends, to form stouter fibers. Images such as those in Figs. 14, 19, and 33 indicate that the crescent fibrils associate into similar sorts of fibers. These associations are unstable in the presence of mica, but whether they involve electrostatic, hydrophobic, or other modes of interaction is unknown. Their constant diameter suggests, however, that they are not random aggregates but rather form in accordance with structural dictates of their component fibrils.

The association of the fibrils into fibers bears directly on our studies of the *C. reinhardi* cell wall, which is composed in part of networks of fibrillar proteins that are biochemically, antigenically, and morphologically related to the fibrils displayed on the flagellar surface (2, 11, 23, 37). We find that in the cell wall, the fibrils also associate into a variety of thicker fibers which dissociate when they contact the mica surface (23). Therefore, the homologies between the wall and the flagellar proteins extend to their mode of interaction in situ.

We thank Brian Gebhart for agglutinin purification, Carol Hwang for cell cultures, Robyn Roth for the replicas, Lori van Houten for photography, Ann Dillon for drawings, and Amy Papiian for typing.

This work was supported by grants GM-26150 to U. W. Goodenough and GM-29647 to J. E. Heuser from the National Institutes of Health.

Received for publication 13 December 1985, and in revised form 13 May 1985.

REFERENCES

- Adair, W. S., C. J. Hwang, and U. W. Goodenough. 1983. Identification and visualization of the sexual agglutinin from the mating-type plus flagellar membrane of *Chlamydomonas*. *Cell*. 33:183-193.
- Cooper, J. B., W. S. Adair, R. P. Mecham, J. E. Heuser, and U. W. Goodenough. 1983.

- Chlamydomonas* agglutinin is a hydroxyproline-rich glycoprotein. *Proc. Natl. Acad. Sci. USA*. 80:5898-5901.
- Lampert, D. T. A. 1980. Structure and function of plant glycoproteins. In *The Biochemistry of Plants*. J. Preiss, editor. Academic Press, Inc. New York. Vol. 3. 501-541.
- Trelstad, R. L. 1984. The Role of Extracellular Matrix in Development. Alan R. Liss, Inc., New York. 642 pp.
- Heuser, J. E. 1980. Three-dimensional visualization of coated vesicle formation in fibroblasts. *J. Cell Biol.* 84:560-583.
- Heuser, J. E. 1983. Procedure for freeze-drying molecules adsorbed to mica flakes. *J. Mol. Biol.* 169:155-195.
- Martin, N. C., and U. W. Goodenough. 1975. Gametic differentiation in *Chlamydomonas reinhardtii*. I. Production of gametes and their fine structure. *J. Cell Biol.* 67:587-605.
- Gorman, D. S., and R. P. Levine. 1965. Cytochrome f and plastocyanin: their sequence in the photosynthetic electron transport chain of *C. reinhardtii*. *Proc. Natl. Acad. Sci. USA*. 54:1565-1569.
- Adair, W. S., B. C. Monk, R. Cohen, and U. W. Goodenough. 1982. Sexual agglutinins from the *Chlamydomonas* flagellar membrane. Partial purification and characterization. *J. Biol. Chem.* 257:4593-4602.
- Collin-Osdoby, P., and W. S. Adair. 1985. Characterization of the purified *Chlamydomonas minus* agglutinin. *J. Cell Biol.* 101:1144-1152.
- Collin-Osdoby, P., W. S. Adair, and U. W. Goodenough. 1984. *Chlamydomonas* agglutinin conjugated to agarose beads as an *in vitro* probe of adhesion. *Exp. Cell Res.* 150:282-291.
- Witman, G. B., K. Carlson, J. Berliner, and J. L. Rosenbaum. 1972. *Chlamydomonas* flagella. I. Isolation and electrophoretic analyses of microtubules, matrix, membranes, and mastigonemes. *J. Cell Biol.* 54:507-539.
- Mesland, D. A. M., and H. van den Ende. 1979. The role of flagellar adhesion in sexual activation of *Chlamydomonas eugametos*. *Protoplasma*. 98:115-129.
- Homer, R. B., and K. Roberts. 1979. Glycoprotein conformation in plant cell walls. Circular dichroism reveals a polyproline II structure. *Planta*. 146:217-222.
- Homan, W. 1982. An analysis of the flagellar surface of *Chlamydomonas eugametos* with respect to sexual agglutination. Ph.D. thesis, University of Amsterdam, Amsterdam, Holland.
- Goodenough, U. W., C. Hwang, and A. J. Warren. 1978. Sex-limited expression of gene loci controlling flagellar membrane agglutination in the *Chlamydomonas* mating reaction. *Genetics*. 89:235-243.
- Hwang, C., B. C. Monk, and U. W. Goodenough. 1981. Linkage of mutations affecting *minus* flagellar membrane agglutinability to the *m⁻* mating type locus of *Chlamydomonas*. *Genetics*. 99:41-47.
- Galloway, R. E., and U. W. Goodenough. 1985. Genetic analysis of mating locus-linked mutations in *Chlamydomonas reinhardtii*. *Genetics*. In press.
- Bergman, K., U. W. Goodenough, D. A. Goodenough, J. Jawitz, and H. Martin. 1975. Gametic differentiation in *Chlamydomonas reinhardtii*. II. Flagellar membranes and the agglutination reaction. *J. Cell Biol.* 67:606-622.
- Snell, W. J. 1976. Mating in *Chlamydomonas*: a system for the study of specific cell adhesion. I. Ultrastructural and electrophoretic analysis of flagellar surface components involved in adhesion. *J. Cell Biol.* 68:48-69.
- Bloodgood, R. A., and J. Workman. 1984. A flagellar surface glycoprotein mediating cell-substrate interaction in *Chlamydomonas*. *Cell Motility*. 4:77-87.
- Monk, B. C., W. S. Adair, R. A. Cohen, and U. W. Goodenough. 1983. Topography of *Chlamydomonas*: fine structure and polypeptide components of the gametic flagellar membrane surface and the cell wall. *Planta*. 158:517-533.
- Goodenough, U. W., and J. E. Heuser. 1985. The *Chlamydomonas* cell wall and its constituent glycoproteins analyzed by the quick-freeze, deep-etch technique. *J. Cell Biol.* In press.
- Pierce, M., and C. E. Ballou. 1983. Cell-cell recognition in yeast. *J. Biol. Chem.* 258:3567-3582.
- Julius, D., L. Blair, A. Brake, G. Sprague, and J. Thorner. 1983. Yeast α factor is processed from a larger precursor polypeptide: the essential role of a membrane-bound dipeptidyl aminopeptidase. *Cell*. 32:839-852.
- Politz, J. C., and R. S. Egar. 1984. Overlapping stage-specific sets of numerous small collagenous polypeptides are translated *in vitro* from *Caenorhabditis elegans* RNA. *Cell*. 37:853-860.
- Goodenough, U. W., and D. Jurivich. 1978. Tipping and mating-structure activation induced in *Chlamydomonas* gametes by flagellar membrane antisera. *J. Cell Biol.* 79:680-693.
- Goodenough, U. W., and R. L. Weiss. 1975. Gametic differentiation in *Chlamydomonas reinhardtii*. III. Cell wall lysis and microfilament associated mating structure activation in wild-type and mutant strains. *J. Cell Biol.* 67:623-637.
- Goodenough, U. W., W. S. Adair, E. Caligor, C. L. Forest, J. L. Hoffman, D. A. M. Mesland, and S. Spath. 1980. Membrane-membrane and membrane-ligand interactions in *Chlamydomonas* mating. In *Membrane-Membrane Interactions*. N. B. Gilula, editor. N.Y., Raven Press. 131-152.
- Goodenough, U. W., and J. Thorner. 1983. Sexual differentiation and mating strategies in the yeast *Saccharomyces* and the green alga *Chlamydomonas*. In *Cell Interactions and Development*. K. M. Yamada, editor. John Wiley & Sons, New York. 29-75.
- Lewin, R. A. 1952. Studies on the flagella of algae. I. General observations on *Chlamydomonas moewusii* Gerloff. *Biol. Bull.* 103:74-79.
- Bloodgood, R. A. 1977. Motility occurring in association with the surface of the *Chlamydomonas* flagellum. *J. Cell Biol.* 75:983-989.
- Hoffman, J. L., and U. W. Goodenough. 1980. Experimental dissection of flagellar surface motility in *Chlamydomonas*. *J. Cell Biol.* 86:656-667.
- Bloodgood, R. A., and G. S. May. 1982. Functional modification of the *Chlamydomonas* flagellar surface. *J. Cell Biol.* 93:88-96.
- Dentler, W. L., M. M. Pratt, and R. E. Stephens. 1980. Microtubule-membrane interactions in cilia. II. Photochemical cross-linking of bridge structures and the identification of a membrane-associated dynein-like ATPase. *J. Cell Biol.* 84:381-403.
- Sattler, C. A., and L. A. Staehelin. 1974. Ciliary membrane differentiations in *Tetrahymena pyriformis*. *Tetrahymena* has four types of cilia. *J. Cell Biol.* 62:473-490.
- Musgrave, A., P. de Wildt, R. Broekman, and H. van den Ende. 1983. The cell wall of *Chlamydomonas eugametos*. Immunological aspects. *Planta*. 158:82-89.